Journal of Structural Geology 166 (2023) 104777

Contents lists available at ScienceDirect

Journal of Structural Geology

journal homepage: www.elsevier.com/locate/jsg

$^{40}Ar/^{39}Ar$ constraints on the tectonic evolution of the central part of the Mesoproterozoic Sveconorwegian orogen

Thomas Scheiber [a,*], Giulio Viola [b,**], Morgan Ganerød [c], Bernard Bingen [c]

[a] Department of Environmental Sciences, Western Norway University of Applied Sciences, Røyrgata 6, 6856, Sogndal, Norway
[b] Department of Biological, Geological and Environmental Sciences, University of Bologna, Via Zamboni 67, 40126, Bologna, Italy
[c] Geological Survey of Norway, Leiv Eirikssons vei 39, 7040, Trondheim, Norway

ARTICLE INFO

Keywords:
Structural analysis
$^{40}Ar/^{39}Ar$ geochronology
Sveconorwegian orogen
Kongsberg lithotectonic unit
Detachment faulting
Orogenic collapse

ABSTRACT

Structural data combined with $^{40}Ar/^{39}Ar$ geochronology of hornblende, muscovite, biotite and plagioclase from 37 localities along three transects allow the time-constrained reconstruction of the Sveconorwegian deformation and cooling history of the Kongsberg lithotectonic unit and of the boundary zone to the adjacent Telemark lithotectonic unit in southern Norway. The Kongsberg lithotectonic unit consists of pervasively deformed, steeply dipping amphibolite-to granulite-facies gneisses, in which Mesoproterozoic $^{40}Ar/^{39}Ar$ ages of c. 1090-1070 Ma record cooling and exhumation. Ages scattering around 1000 Ma are interpreted as resetting of the K/Ar systems related to sinistral strike-slip deformation along c. N–S trending greenschist-to amphibolite facies shear zones and associated large-scale folding. Later, Neoproterozoic top-to-the-E normal shearing accommodated by the newly discovered Prestfoss detachment selectively exploiting the Kongsberg-Telemark boundary zone caused the exhumation of amphibolite-facies rocks of the Telemark lithotectonic unit and their juxtaposition against amphibolite-facies gneisses of the Kongsberg lithotectonic unit, which had cooled earlier in the orogenic history. $^{40}Ar/^{39}Ar$ ages constrain shearing and associated cooling to between c. 940 Ma and c. 900 Ma. Finally, a Silurian (420 ± 11 Ma) $^{40}Ar/^{39}Ar$ age may reflect localized partial to complete resetting due to Caledonian tectonics, and a Permian (288 ± 1 Ma) $^{40}Ar/^{39}Ar$ age constrains the intrusion of an Oslo Rift granite.

1. Introduction

The unravelling of the crustal dynamics of ancient and deeply eroded orogens is commonly hindered by the lack of sufficient lithological, structural and temporal markers to allow straightforward, local or regional correlations and tectonic reconstructions. In turn, this commonly compromises the successful deconvolution of the complex current and past geological relationships among crustal blocks or terranes that are juxtaposed along structural contacts because of long and multiphase orogenic evolutions.

High-resolution structural and metamorphic studies can shed light on the geometry, kinematics and grade of deformation accommodated along orogen-scale faults or shear zones and of the juxtaposed blocks (e.g., Anczkiewicz et al., 2007; Bodorkos and Clark, 2004; Goscombe and Gray, 2008; Holdsworth and Pinheiro, 2000; Viola et al., 2008). However, even in the presence of such detailed studies, much of the evolutionary history of deeply exhumed orogens remains generally unknown or poorly constrained, particularly with respect to the late orogenic exhumation of individual crustal blocks to upper crustal conditions during final orogen structuring and its later tearing down. The orogenic tectonothermal history of the assembly of crustal units may, however, be efficiently explored by an integrated approach combining detailed thermochronological studies along transects straddling the main shear zones of the orogen with detailed structural analysis of the individual lithotectonic domains. Particularly in the case of ancient orogens, detailed structural analyses are generally complex due to the many likely episodes of both ductile and brittle structural reactivation (e.g., Holdsworth et al., 2001; Scheiber et al., 2015; Viola et al., 2009).

The Sveconorwegian orogen of southern Scandinavia is a good example of a deeply exhumed orogenic system that experienced a

Abbreviations: LTU, lithotectonic unit; KTBZ, Kongsberg-Telemark boundary zone.

* Corresponding author. Røyrgata 6, 6856, Sogndal, Norway.
** Corresponding author. Via Zamboni 67, 40126, Bologna, Italy.
E-mail addresses: thomas.scheiber@hvl.no (T. Scheiber), giulio.viola3@unibo.it (G. Viola), morgan.ganerod@ngu.no (M. Ganerød), bernard.bingen@ngu.no (B. Bingen).

https://doi.org/10.1016/j.jsg.2022.104777
Received 4 March 2022; Received in revised form 14 December 2022; Accepted 16 December 2022
Available online 21 December 2022

complex and long history of crustal amalgamation and deformation during multiple orogenic stages (Bingen et al., 2008b, 2021; Möller and Andersson, 2018; Slagstad et al., 2020; Stephens et al., 2020). Geochronological studies (predominantly U–Pb dating on zircon) have so far constrained the details of the orogen's local magmatic and sedimentary history and, only to a lesser extent, of the metamorphic evolution of its constituent lithotectonic units (LTUs). Direct dating of both ductile and brittle deformation and of the associated tectonic exhumation is scarce in the Sveconorwegian orogen, preventing detailed and time-constrained correlations and reconstructions of the orogen evolution in time and space.

Aiming to help bridge this gap, in this paper we:

(1) assess the hitherto largely unknown regional thermal histories within the Kongsberg LTU of southern Norway and their spatial variations. To this end, we present a regional geochronological study based on sixty new apparent $^{40}Ar/^{39}Ar$ age results on amphibole, white mica, biotite, K-feldspar and plagioclase.
(2) add constraints to the deformation history of several large, orogen-scale shear zones that are either contiguous to- or directly deform the Kongsberg LTU.

The differential exhumation detected across orogen-scale shear zones may be used in combination with structural analyses to unravel the complete thermal and structural evolution of the tectonic boundaries of the studied lithotectonic domains, thus improving the understanding of the evolution of the deeply exhumed Sveconorwegian orogen. Results of this study integrate the structural analysis by Scheiber et al. (2015), who elaborated a field-based structural model for the long-lived structural evolution of the Kongsberg LTU. Data were collected during the KONGMO mapping project hosted by the Geological Survey of Norway and synthesized in the 1:100 000 bedrock map by Viola et al. (2016). Finally, our results are discussed in the larger framework of the Sveconorwegian orogen.

2. Geological outline

The southwestern Baltican Shield consists of crustal domains accreted during the late Meso-to Neoproterozoic Sveconorwegian orogeny between c. 1140 and 920 Ma (Fig. 1a). This mountain-building orogeny juxtaposed crustal domains characterized by different tectonometamorphic styles with complex and multiphase deformation histories spanning more than 200 Ma (Bingen et al., 2008b, 2021; Möller and Andersson, 2018; Slagstad et al., 2020; Stephens et al., 2020). The constituent crustal domains have been traditionally separated into distinct lithotectonic units (LTUs) based on (i) their paleogeography and lithological composition, (ii) their metamorphic signatures, (iii) the timing of (high-grade) metamorphic events and (iv) intervening orogen-scale shear zones. Early Sveconorwegian (1145–1080 Ma) convergence and high-grade metamorphism in the central parts of the orogen (Kongsberg and Bamble LTUs) were followed by high-pressure metamorphism at c. 1050 in the Idefjorden LTU and at c. 990 Ma in the Eastern Segment (Fig. 1b; Bingen et al., 2008a; Möller et al., 2015). In the western part of the Sveconorwegian realm, orogenic magmatism took place at 1070–1010 Ma (Slagstad et al., 2018), culminating in ultra-high-temperature metamorphism (Blereau et al., 2017; Laurent et al., 2018). Younger (990-915 Ma) magmatism is recorded predominantly in the western (hornblende-biotite granitoid suite; Andersen et al., 2002; Granseth et al., 2020; Vander Auwera et al., 2011) and central part (Bohus-Flå granite belt; Andersson et al., 1996; Eliasson and Schöberg, 1991; Lamminen et al., 2011) of the orogen (Fig. 1b). In the following, the Kongsberg and neighbouring LTUs (Fig. 2) are described in more detail while also providing a succinct characterization of the tectonic boundary zone separating the Kongsberg and Telemark LTU's.

2.1. The Kongsberg LTU

The Kongsberg LTU is internally subdivided into the Kongsberg and Modum complexes (Fig. 2a). The Kongsberg complex mainly consists of metaplutonic rocks with intercalations of metavolcanic and

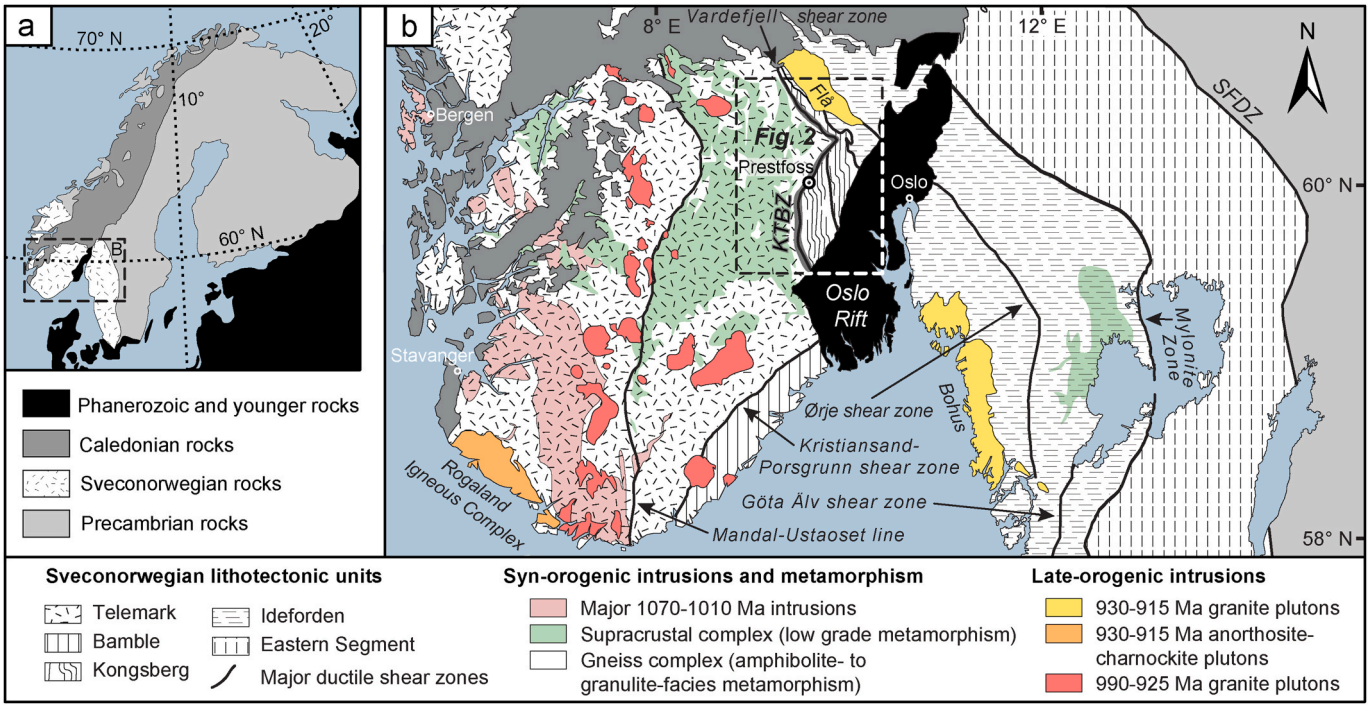

Fig. 1. (a) Tectonic map of Fennoscandia. (b) Simplified lithotectonic framework of the Sveconorwegian orogen of southern Norway and Sweden (modified after Viola and Henderson, 2010) showing (1) major tectonic boundaries separating lithotectonic units, (2) the distribution of gneiss vs. supracrustal complexes and major syn-orogenic intrusions (after Bingen et al., 2021), and (3) major late-to post-orogenic intrusions. Abbreviations: KTBZ, Kongsberg Telemark boundary zone; SFDZ, Sveconorwegian frontal deformation zone.

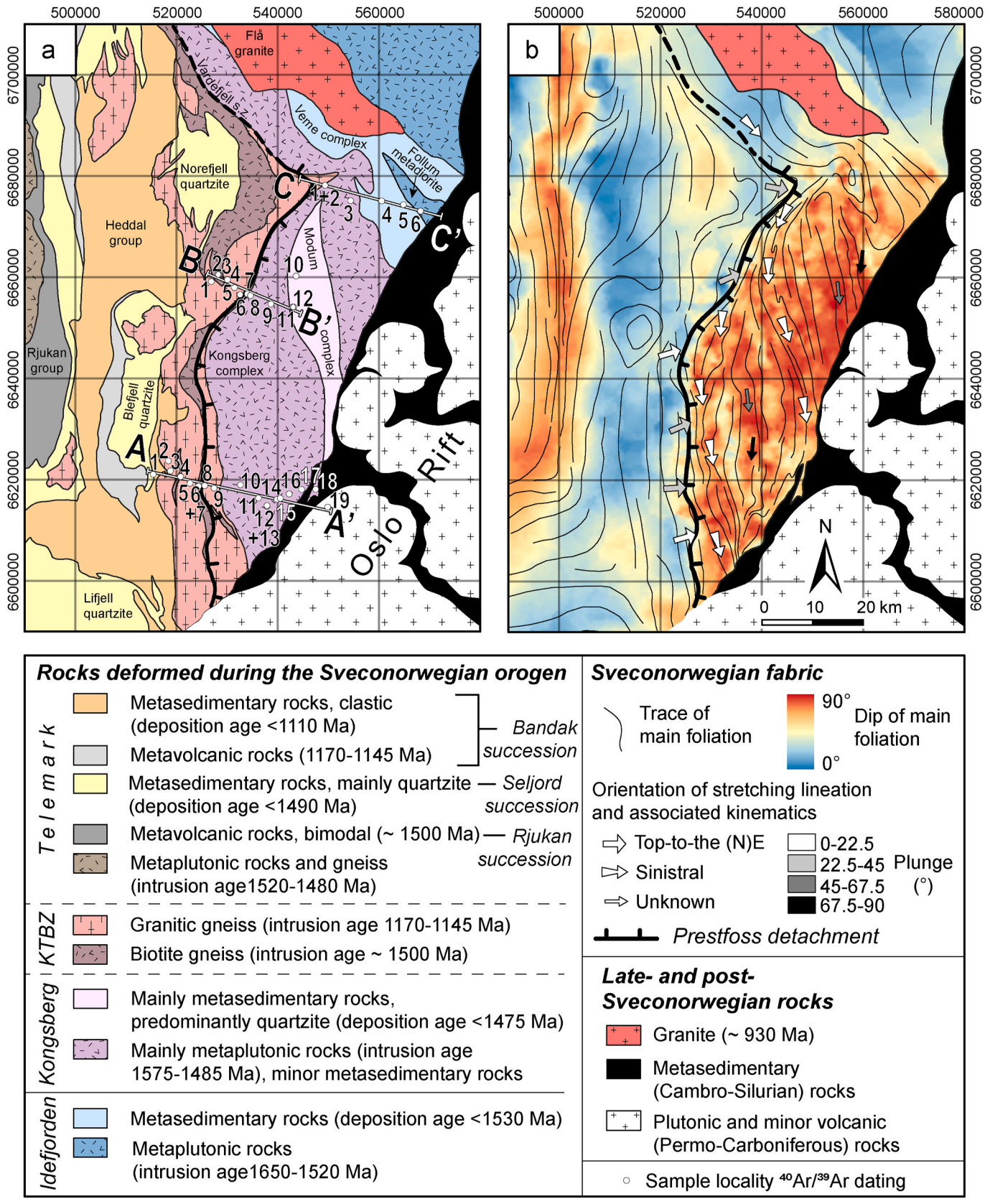

Fig. 2. (a) Map of the Kongsberg lithotectonic unit, the adjacent Telemark lithotectonic unit to the west and the Idefjorden lithotectonic unit to the northeast. Maximum ages of deposition correspond to youngest detrital zircon ages (see compilation in Bingen and Viola, 2018). $^{40}Ar/^{39}Ar$ sampling locations are indicated in each of the three transects and traces of cross sections (Fig. 7) are shown. (b) Structural architecture of these Sveconorwegian LTUs shown by a foliation trace map combined with surface variations of dip angle (kriging interpolation). Interpolation based on 17 323 foliation measurements.

metasedimentary sequences. The orthogneisses of the Kongsberg complex yield U–Pb zircon crystallization ages between 1575 and 1485 Ma, with a peak at c. 1505 Ma (Andersen et al., 2004; Bingen and Viola, 2018). The Modum complex is, instead, predominantly made of a quartz-rich metasedimentary succession with a maximum depositional age of c. 1470 Ma (U–Pb detrital zircon age) and most probably represents remnants of the epicontinental cover sequence of the Kongsberg complex basement (Bingen et al., 2001). Meta-gabbroic bodies hosted by both the Kongsberg and Modum complexes yield U–Pb zircon and Sm–Nd mineral ages that constrain two episodes of magmatic crystallization at c. 1575-1485 Ma and at 1210-1140 Ma (Bingen and Viola, 2018; Munz et al., 1994). The Kongsberg LTU is characterized by early Sveconorwegian amphibolite-facies metamorphism in the southwest grading to upper amphibolite-facies conditions in the Modum complex and granulite-facies metamorphism in the eastern Kongsberg complex (Table 1 and references given in the table). Regional peak amphibolite-facies metamorphism associated with partial melting has been constrained to c. 1145-1130 Ma (U–Pb ages on metamorphic zircon; Bingen and Viola, 2018). Younger ages between 1120 and 1080 Ma are also reported in the same study and earlier studies (mainly zircon, monazite and titanite U–Pb ages) and interpreted to constrain retrograde metamorphism and metasomatism (Table 1, Andersen and Grorud, 1998; Bingen et al., 2001; Bingen et al., 2008a; Munz et al., 1994).

2.2. The eastern telemark LTU

The eastern part of the Telemark LTU (Fig. 1b) is characterized by greenschist-to amphibolite facies supracrustal rocks overlying polymetamorphic gneiss complexes (Brewer and Menuge, 1998; Starmer, 1993). The Telemark supracrustal rocks still preserve primary sedimentary and volcanic structures and several unconformities (Köykkä, 2011a, b; Lamminen, 2011; Laajoki et al., 2002), and have been separated into three successions, which, from bottom to top, are the Rjukan, Seljord and Bandak successions (cf. review in Bingen et al., 2021). The Lifjell, Blefjell and Norefjell quartzites (Fig. 2a) form part of the Seljord succession and are generally related to pre-Sveconorwegian continental-margin extension (Köykkä and Lamminen, 2011; Lamminen and Köykkä, 2010). These quartzites were deformed under amphibolite-facies conditions during the Sveconorwegian orogeny (Brewer and Atkin, 1987; Köykkä and Lamminen, 2011; Lamminen and Köykkä, 2010). The metasedimentary rocks of the Heddal group (Fig. 2a) belong to the Bandak succession and were deposited at or after c. 1110 Ma (U–Pb detrital zircon data), i.e., only after the onset of the Sveconorwegian orogeny (Bingen et al., 2003; Köykkä, 2011a; Spencer et al., 2014).

2.3. The Kongsberg-Telemark boundary zone (KTBZ)

The tectonic boundary between the Kongsberg and Telemark LTUs corresponds to an up to 10 km thick deformation zone (Fig. 1b) that accommodated strain under different metamorphic conditions and at

Table 1
Summary of previous geochronological and petrological studies.

Geologic context	Method	Analyzed material	Interpretation	P-T peak value	Age (Ma)	Reference
Kongsberg complex	U–Pb	zircon	amphibolite to granulite-facies metamorphism		1156 ± 26 to 1090 ± 23 (6 ages)	Bingen and Viola (2018)
Kongsberg complex (Vardefjell shear zone)	U–Pb	zircon	metamorphism		1012 ± 7, 1008 ± 14	Bingen et al. (2008a)
Kongsberg complex (Vardefjell shear zone)	U–Pb	titanite	metamorphism		985 ± 5	Bingen et al. (2008a)
Kongsberg complex	U–Pb	zircon	lamprophyric dyke intrusion		1033 ± 5	Bingen and Viola (2018)
Modum complex	Pb/Pb	uraninite	localized hydrothermal reworking		1146 ± 66	Andersen and Grorud (1998)
Modum complex	Re–Os	molybdenite	metamorphism		1112 ± 4	Bingen et al. (2008a)
Modum complex	U–Pb	monazite	metamorphism		1092 ± 1	Bingen et al. (2008a)
Modum complex	U–Pb	titanite	albitization		1080 ± 3	Munz et al. (1994)
Modum complex	U–Pb	zircon	metamorphism		1102 ± 28	Bingen et al. (2001)
Modum complex	Pb/Pb	whole rock	uranium metasomatism		1060 ± 73	Andersen and Munz (1995)
Modum complex	K–Ar	phlogopite	pegmatite intrusion		1041	Neumann (1960)
KTBZ	U–Pb	zircon	metamorphism		1014 ± 1	Bingen et al. (2008a)
KTBZ	K–Ar	biotite			852	Neumann (1960)
KTBZ	K–Ar	sericite			895	Neumann (1960)
KTBZ	K–Ar	muscovite	pegmatite intrusion		977	Neumann (1960)
KTBZ	K–Ar	mica			990	Neumann (1960)
Idefjorden LTU	K–Ar	muscovite			1052	Neumann (1960)
Idefjorden LTU	K–Ar	biotite			1048	Neumann (1960)
Modum complex	thermobarometry	metagabbro	metamorphism, formation of corona textures	7–8 kbar, 600–800 °C		Munz and Morvik (1991)
Modum complex	thermobarometry	whiteschist	hydrothermal alteration	6–8 kbar, 600–750 °C		Munz (1990)
Modum complex	petrology	coronitic gabbro	metamorphism (amphibolite- to pumpellyite-prehnite facies) and metasomatism (scapolitization and albitization)			Austrheim et al. (2008)

different times (Scheiber et al., 2015). This boundary zone generally strikes N–S to NE-SW, dips towards the E/SE in its southern part but turns into an NW-SE trend and acquires a gentle SW dip in the northern part, where it is known as the Vardefjell Shear Zone (Figs. 1b and 2a; Bingen et al., 2008a). In the study area, this shear zone mainly cuts across a belt of granitic gneiss with U–Pb zircon intrusion ages ranging from 1170 to 1145 Ma (Bingen et al., 2003; Scheiber et al., 2015) and a biotite-bearing orthogneiss with U–Pb zircon age of c. 1500 Ma interpreted as crystallization age of the rock (Bingen and Viola, 2018). These rocks have traditionally been interpreted as part of the eastern Telemark LTU (Nordgulen, 1999). Their deformation occurred at amphibolite facies metamorphic conditions and has been constrained to between c. 1010 Ma and 985 Ma (U–Pb zircon and titanite ages, respectively; Bingen et al., 2008a; Bingen and Viola, 2018). These ages were interpreted to constrain local sinistral shearing along the immediate contact to the Kongsberg complex (Scheiber et al., 2015). Similarly, sinistral shear kinematics are also recorded along a large-scale shear zone within the Kongsberg LTU (Fig. 1b), where it overprints an older (early-Sveconorwegian) regional amphibolite-to granulite-facies fabric characterized by steeply plunging lineations (Fig. 2b). Top-to-the-E extension-related fabrics along the newly discovered Prestfoss detachment (Fig. 2; see below) overprint and truncate the sinistral shear fabric towards the western part of the KTBZ, as discussed below.

2.4. The Idefjorden LTU

The Idefjorden LTU contains Paleo-to Mesoproterozoic (1650-1520 Ma) plutonic and volcanic rocks in addition to two metasedimentary sequences, referred to as the Veme and the Stora Le-Marstrand complexes, which are correlatives west and east of the Oslo rift, respectively (Figs. 1b and 2a) (Bingen et al., 2001). The Veme complex comprises thick packages of amphibolite-facies turbiditic metapsammite and metagreywacke with a maximum deposition age of c. 1530 Ma (U–Pb detrital zircon data; Bingen et al., 2001). The Veme complex hosts the Follum metadiorite (Fig. 2b), which belongs to the plutonic suite of the Idefjorden LTU and has a U–Pb zircon intrusion age of c. 1555 Ma (Bingen et al., 2005).

3. $^{40}Ar/^{39}Ar$ geochronology: sampling strategy and methodology

Thirty-seven samples of generally coarse-grained rock types were collected from along three profiles straddling the KTBZ and crossing the Kongsberg LTU at different latitudes (A-A′, B–B′ and C–C′ in Fig. 2a). Separation and dating of multiple mineral phases resulted in a geochronological dataset consisting of sixty new $^{40}Ar/^{39}Ar$ dates (nineteen amphibole, thirty-two biotite, four muscovite, four plagioclase dates and one K-Feldspar date) (Table 2). Sampling was carried out aiming at the clarification of the regional cooling pattern of the Kongsberg LTU and of the adjacent Telemark LTU. Additionally, we aimed at resolving how the study area was affected by the long-lasting tectonic activity of the KTBZ, and by a possible thermal overprint during the Caledonian orogeny and the evolution of the Permian Oslo Rift. Petrographic thin section analysis was used to confirm mineral purity and to establish textural and microstructural relationships between the different mineral phases of each dated sample.

Samples were crushed, grinded and subsequently sieved to obtain 180–250 μm fractions. The mineral separates were washed in acetone and deionized water several times and handpicked under a stereomicroscope. Mineral grains with coatings or inclusions were avoided. Samples (in the form of aliquots of several grains) were packed in aluminium capsules bracketed by the Hb3gr amphibole flux monitor standard (batch PP20) along with pure (zero age) K_2SO_4 and CaF_2 salts. The samples were irradiated at IFE (Institutt for Energiteknikk, Kjeller, Norway) in two different irradiation batches with a nominal neutron flux of 1.3×10^{13} n*(cm^{-2} *s^{-1}). The correction factors for the production of isotopes from Ca and K can be found in supplementary data. The samples were step heated using either a defocused Merchantek CO_2 laser or a double vacuum furnace (Heine type) equipped with a thermocouple (Type C). The extracted gases were passed over SAES GP-50 getters for the first 2 min, then for 9 min in a separate part of the extraction line with SAES AP-10 getters. They were analyzed with an automated MAP 215–50 mass spectrometer in static mode, installed at the Geological Survey of Norway. The peaks were determined during peak hopping for 10 cycles (15 integrations per cycle) on the different masses ($^{40–36}Ar$) on an analouge Balzers electron multiplier and regressed back to zero inlet time. Blanks were analyzed after every third measurement of an unknown. After blank correction, a correction for mass fractionation, ^{37}Ar and ^{39}Ar decay and neutron-induced interference reactions produced in the reactor was undertaken using in-house software. It implements the equations of McDougall and Harrison (1999) and the proposed decay constant for ^{40}K after Renne et al. (2010). A $^{40}Ar/^{36}Ar$ ratio of 298.56 ± 0.31 (±1σ) (Lee et al., 2006), was used for the atmospheric argon correction and mass fractionation calculation (power law). We calculated J-values relative to an age of 1080.4 ± 1.1 (±1σ) Ma for the Hb3gr hornblende flux monitor (Renne et al., 2010). Weighted mean plateau ages (WMPA) and weighted mean ages (WMA) were calculated for consecutive identical steps by weighting on the inverse of the variance (analytical uncertainties), where a plateau is defined as comprising more than 50% of the released ^{39}Ar (WMPA). All ages are reported at the 1.96σ confidence level. We follow the general guidelines presented in Schaen et al. (2020) aiming at a standardized presentation and interpretation of $^{40}Ar/^{39}Ar$ ages.

Our geochronological raw data and all degassing spectra and associated inverse isochrons are reported in the journal electronic repository (supplementary data). Based on the individual degassing spectra, the analytical quality of each calculated date was assessed (cf. supplementary data and Table 2): Weigthed mean (plateau) ages with MSWD (mean square weighted deviation) values between 0.1 and 2.7 are considered of statistical significance (bold ages in Table 2 and supplementary data), and the degassing spectra of these ages are presented in Figs. 3–5. For sample A-18 (amphibole) we prefer to report the inverse isochron age (Fig. 3o), which, in this particular case, is statistically more robust than the associated WMA. In five samples, it was possible to derive two WMAs from a single spectrum (A-7 plagioclase, B5, B8, B12 biotite, C5 biotite). The obtained WMAs from each spectrum generally plot in a similar age range, and, therefore, we interpret the WMA including more released ^{39}Ar and/or exhibiting a MSWD closer to 1 as that of higher statistical significance.

In summary, 37 dates are interpreted as being statistically robust (Table 2, Figs. 3–5) and are further reported and discussed in this paper.

4. Results

The new structural and geochronological results are presented separately from the three transects, from south to north. In this chapter, representative structural data are provided in a simplified synoptic map (Fig. 2b), as field impressions (Fig. 6), geological cross sections (Fig. 7) and microphotographs (Fig. 8). For each transect, the presentation of the structural framework is followed by an integrated description of the geochronological results. Thereafter, microfabrics of the dated samples for each structural domain are presented before a summary view of the many obtained results.

4.1. Transect A-A'

This transect covers the entire Kongsberg LTU. It starts in the WNW in the Telemark LTU, in a quartzite supracrustal unit (the Blefjell quartzite, Fig. 2) and runs across the 1170-1145 Ma granitic gneiss belt (Figs. 2a and 7a) which, together with the c. 1500 Ma biotite gneiss, makes up the KTBZ. In the WNW part of the transect, an amphibolite-facies foliation is subhorizontal and, as one approaches the KTBZ, it

Table 2
Summary of $^{40}Ar/^{39}Ar$ data.

Sample ID	Original sample ID	Sample locality (UTM 32V)		Rock type	Geologic context	Mineral	TFA	Spectrum[a]			Inverse isochron		
		X	Y					Σ^{39}Ar%	Age[b]	MSWD	Age[b]	MSWD	$^{40}Ar/^{36}Ar$
A-1	GVI_50	515393	6621053	Biotite-muscovite layer in quartzite	Blefjell quartzite	biotite	891 ± 1	45	**906 ± 2**	0.8	905 ± 4	1.0	310 ± 32
						muscovite	889 ± 1	76	**890 ± 1**	1.2	891 ± 2	0.04	158 ± 178
A-2	GVI_51	518086	6622136	Biotite-amphibole granitic gneiss	KTBZ granite gneiss	biotite	875 ± 3	68	**889 ± 5**	0.6	901 ± 2	0.2	-1553 ± 3634
A-3	GVI_52	518781	6621719	Biotite-amphibole granite	KTBZ granite gneiss	K-feldspar	713 ± 4	-	-	-	-	-	-
A-4	GVI_53	520790	6620602	Mafic dyke	KTBZ	amphibole	950 ± 14	77	**958 ± 15**	0.1	-	-	-
						plagioclase	526 ± 2	-	-	-	383 ± 47	69.2	2929 ± 1517
A-5	GVI_54	522672	6619295	Biotite-amphibole granitic gneiss	KTBZ granite gneiss	biotite	655 ± 9	-	-		-	-	-
A-6	GVI_55	524468	6618816	Biotite-amphibole granitic gneiss	KTBZ granite gneiss	biotite	617 ± 40	-	-	-	626 ± 142	19.8	305 ± 19
A-7	GVI_56	524438	6618808	Mafic dyke	KTBZ granite gneiss	amphibole	942 ± 4	-	-	-	-	-	-
						plagioclase	427 ± 3	70	386 ± 11	91.1	410 ± 14	16.6	-225 ± 261
						plagioclase	427 ± 3	19	**420 ± 11**	1.2	342 ± 186	0.2	1349 ± 3612
A-8	GVI_57	525577	6618824	Biotite-amphibole granitic gneiss	KTBZ granite gneiss	biotite	848 ± 6	44	**981 ± 16**	2.4	934 ± 15	0.04	266 ± 29
A-9	GVI_58	527403	6618321	Amphibole-biotite granitic gneiss	KTBZ granite gneiss	amphibole	1050 ± 2	-	-	-	-	-	-
						biotite	997 ± 1	87	1019 ± 19	230.3	1054 ± 8	4.1	-3342 ± 854
A-10	GVI_59	532624	6618982	Garnet-biotite gneiss	Kongsberg complex	biotite	1007 ± 6	96	**1015 ± 5**	1.6	1010 ± 11	1.6	316 ± 34
A-11	GVI_60	536191	6616358	Amphibole-biotite dioritic gneiss	Kongsberg complex	amphibole	1085 ± 9	82	**1089 ± 3**	0.1	1093 ± 17	0.01	-127 ± 1412
A-12	GVI_61	537870	6614749	Amphibole-biotite dioritic gneiss	Kongsberg complex	biotite	1062 ± 3	-	-	-	1099 ± 97	1183.2	310 ± 52
						amphibole	1000 ± 23	-	-	-	972 ± 178	227.7	292 ± 36
A-13	GVI_62	537865	6614733	Muscovite-biotite phyllonite	Kongsberg complex	biotite	1174 ± 4	64	**1245 ± 4**	1.1	1253 ± 9	0.2	195 ± 117
A-14	GVI_63	539850	6616121	Amphibole dioritic gneiss	Kongsberg complex	amphibole	1106 ± 14	78	**1089 ± 7**	0.8	1096 ± 18	0.9	276 ± 49
A-15	GVI_64	540501	6616318	Biotite-amphibole dioritic gneiss	Kongsberg complex	amphibole	1065 ± 7	91	**1095 ± 6**	1.0	1095 ± 8	2.0	294 ± 99
A-16	GVI_65	542249	6617188	Biotite-amphibole dioritic gneiss	Kongsberg complex	biotite	1046 ± 6	90	**1056 ± 2**	0.6	1056 ± 2	0.7	299 ± 3
						amphibole	1091 ± 7	86	**1090 ± 2**	0.7	-	-	-
A-17	GVI_66	544722	6618059	Biotite granodioritic gneiss	Kongsberg complex	biotite	1133 ± 16	76	**1151 ± 8**	0.9	1148 ± 9	0.5	311 ± 14
						plagioclase	661 ± 1	-	-	-	-	-	-
A-18	GVI_68	547490	6618101	Biotite augengneiss	Kongsberg complex	biotite	658 ± 2	-	-	-	657± 14	150.6	302 ± 21
						amphibole	888 ± 6	12	1051 ± 27	4.3	**1071 ± 19**	1.0	247 ± 36
A-19	GVI_69	549873	6614583	Amphibole granite	Oslo Rift	amphibole	285 ± 3	70	**288 ± 1**	1.0	287 ± 1	1.3	300 ± 5
B-1	GVI_72	526861	6659128	Biotite-amphibole granitic gneiss	KTBZ granitic gneiss	biotite	923 ± 19	73	**885 ± 7**	0.1	884 ± 8	0.1	358 ± 356
B-2	GVI_70	528439	6660448	Granodiorite gneiss	KTBZ biotite gneiss	biotite	910 ± 4	43	**924 ± 6**	2.7	941 ± 15	0.001	-26 ± 275
						amphibole	920 ± 2	73	**928 ± 1**	1.6	912 ± 21	0.7	3724 ± 5222
B-3	GVI_71	528439	6660448	Felsic layer	KTBZ biotite gneiss	biotite	800 ± 12	-	-	-	-	-	-
						amphibole	904 ± 1	92	908 ± 10	65.6	940 ± 32	48.9	-382 ± 364
B-4	GVI_73	530054	6659484	Biotite-amphibole granitic gneiss	KTBZ granitic gneiss	biotite	892 ± 1	93	919 ± 10	401.4	926 ± 11	319.2	217 ± 66
						amphibole	942 ± 3	79	**946 ± 2**	1.5	941 ± 7	0.2	1381 ± 1416
B-5	GVI_74	531448	6657952	Biotite granitic gneiss	KTBZ granitic gneiss	biotite	902 ± 1	40	**902 ± 1**	1.2	900 ± 2	0.1	530 ± 295
						biotite	902 ± 1	31	909 ± 1	0.3	911 ± 8	0.4	90 ± 190
B-6	GVI_75	532560	6656562	Biotite granitic gneiss	KTBZ granitic gneiss	biotite	896 ± 2	77	**907 ± 2**	0.5	903 ± 6	0.2	382 ± 137
						amphibole	980 ± 3	29	**915 ± 4**	1.0	922 ± 27	1.8	57 ± 111
B-7	GVI_76	533986	6656680	Protocataclastic granitic gneiss	KTBZ granitic gneiss	amphibole	717 ± 3	-	-	-	-	-	-
B-8	GVI_77	534618	6656363	Biotite schist	Kongsberg complex	biotite	974 ± 4	25	973 ± 3	0.6	972 ± 3	0.3	300 ± 2
						biotite	974 ± 4	60	**995 ± 3**	0.8	994 ± 4	0.9	303 ± 26
B-9	GVI_78	538656	6654705	Amphibole-biotite gneiss	Kongsberg complex	biotite	1020 ± 2	61	**1020 ± 1**	0.1	1023 ± 16	0.1	-32 ± 163
						amphibole	1071 ± 3	93	**1074 ± 2**	0.6	1072 ± 5	0.2	419 ± 211
B-10	GVI_79	543619	6660222	Amphibole-biotite granite	Modum complex	biotite	1004 ± 3	52	1100 ± 3	82.0	-	-	-
						amphibole	993 ± 1	-	-	-	1066 ± 52	114.4	-1509 ± 2908
B-11	GVI_87	542977	6654105	Feldspar-biotite schist	Modum complex	biotite	1076 ± 3	95	**1078 ± 1**	0.3	1078 ± 5	0.4	323 ± 493
B-12	GVI_86	543014	6654079	Quartzite	Modum complex	biotite	988 ± 2	42	996 ± 1	0.3	996 ± 3	0.5	298 ± 19
						biotite	988 ± 2	45	**1011 ± 3**	1.3	1010 ± 7	1.7	374 ± 299
						muscovite	1015 ± 3	95	**1015 ± 3**	1.2	1014 ± 3	1.3	390 ± 170
C-1	GVI_84	549351	6678147	Garnet-biotite gneiss	Kongsberg complex	biotite	972 ± 35	51	1039 ± 55	1.3	-	-	-

(*continued on next page*)

Table 2 (*continued*)

Sample ID	Original sample ID	Sample locality (UTM 32V)		Rock type	Geologic context	Mineral	TFA	Spectrum[a]			Inverse isochron		
		X	Y					Σ^{39}Ar%	Age[b]	MSWD	Age[b]	MSWD	^{40}Ar/^{36}Ar
C-2	GVI_85	549351	6678147	Felsic layer	Kongsberg complex	biotite	963 ± 5	41	**989 ± 7**	0.3	994 ± 16	0.1	259 ± 111
						muscovite	990 ± 2	89	**991 ± 1**	0.6	991 ± 2	0.8	286 ± 236
C-3	GVI_83	554393	6675114	Amphibolite	Kongsberg complex	amphibole	1030 ± 7	77	**1029 ± 5**	1.5	1047 ± 20	0.1	-124 ± 400
C-4	GVI_82	560528	6675055	Amphibole-biotite gneiss	Verne complex	biotite	1004 ± 7	90	**1015 ± 4**	0.9	-	-	-
C-5	GVI_81	564831	6674320	Biotite-muscovite quartzite	Verne complex	biotite	971 ± 5	47	**971 ± 3**	1.3	971 ± 4	1.8	299 ± 9
						biotite	971 ± 5	41	1007 ± 10	1.4	1014 ± 22	1.7	276 ± 64
						muscovite	978 ± 1	83	**979 ± 1**	0.5	-	-	-
C-6	GVI_80	568217	6673064	(Follum) Metadiorite	Idefjorden gneiss	biotite	1174 ± 74	-	-	-	-	-	-
						amphibole	1055 ± 9	85	**1079 ± 9**	0.6	1080 ± 10	0.9	297 ± 35

TFA, total fusion age; MSWD, mean squared weighted deviation.
[a] WMPA, weighted mean plateau age (>50% cumulative ^{39}Ar); WMA, weighted mean age (<50% cumulative ^{39}Ar).
[b] Ages in Ma, errors reported as ± 1.96 σ

becomes progressively steeper dipping toward the ESE. There, it bears an E-plunging stretching lineation and is associated with diffuse extensional top-to-the-east kinematics (Fig. 6a). Towards the east, this foliation abuts an older subvertical mylonitic shear belt associated with greenschist-to amphibolite facies mineral assemblages. This shear belt is characterized by a shallowly c. S-plunging stretching lineation and sinistral shear kinematics, which deforms the easternmost part of the granitic gneiss and the adjacent Kongsberg LTU (Figs. 2b and 7a). The structural style within the Kongsberg LTU is characterized by large-scale, tight to isoclinal upright folds with shallowly plunging fold axes and variably plunging stretching lineations (Figs. 2b, 6b and 7a). At its eastern termination, the transect crosses the unconformity to the Cambro-Silurian metasedimentary rocks and the Permo-Carboniferous intrusions of the Oslo Rift.

Along this transect, sixteen ^{40}Ar/^{39}Ar ages were obtained from nineteen samples. These ages range from 1245 ± 4 Ma (biotite WMPA from the Kongsberg complex) to 288 ± 1 Ma (amphibole WMPA age from an Oslo Rift granite; Fig. 7a), with the majority of the ages clustering at the Meso-Neoproterozoic boundary between c. 1100 and 900 Ma (Figs. 3 and 7a). The two oldest obtained ages (1245 ± 4 and 1151 ± 8 Ma; both biotite WMPAs; Table 2) are from a phyllonite overprinting amphibolite-facies Sveconorwegian structures and from a 1485 ± 12 Ma granodiorite (U–Pb zircon intrusion age; Bingen and Viola, 2018), respectively. Although both ages derive from well-defined plateaus in the degassing spectra (Fig. 3i, n), they are unexpectedly old as they predate Sveconorwegian deformation. One mafic dike (A-7) within the KTBZ yields a Paleozoic plagioclase WMA of 420 ± 11 Ma age (Fig. 3e). For the Sveconorwegian rocks, there is a clear trend from younger ^{40}Ar/^{39}Ar ages (amphibole, biotite and muscovite, c. 900–950 Ma) in the western part of the transect, coincident with areas dominated by a flat to only gently dipping foliation, to older ages (amphibole and biotite, largely between 1000 and 1100 Ma) in the east within areas characterized by steep foliation attitudes (Figs. 2b and 7a).

4.2. *Transect B–B'*

Transect B–B' runs across the Kongsberg-Telemark boundary zone into the Kongsberg complex and the Modum complex (Figs. 2a and 7b). In the biotite gneiss and the granitic gneiss in the north-western part of this transect, the main foliation is subhorizontal to gently ESE-dipping. Towards the contact to the Kongsberg complex, the main foliation in the granitic gneiss gradually turns into a steeper dip. The foliation in the KTBZ lithologies is characterized by amphibolite facies mineral assemblages and is associated with an easterly plunging stretching lineation (Fig. 2b) and top-to-the-E kinematic indicators which include asymmetric boudinage and E-vergent folds of migmatitic layers (Fig. 6c–d). In the Kongsberg LTU, the greenschist-to amphibolite-facies foliation is vertical to steeply-dipping and the structural style is characterized by tight to isoclinal upright folds with gently plunging c. N–S trending fold axes (Figs. 6e and 7b). The gently SSW plunging to subhorizontal stretching lineation is subparallel to the fold axes; kinematic indicators such as asymmetric clasts or lenses and folded competent layers indicate a sinistral sense of shear (Fig. 6f).

Thirteen ^{40}Ar/^{39}Ar step-heating ages were obtained from twelve samples from along transect B–B' (Fig. 4). Six samples are from the KTBZ granitic gneiss and biotite gneiss, two from the Kongsberg complex and three from the Modum complex. The boundary between the granitic gneiss and the Kongsberg LTU is associated with a clear change of the ^{40}Ar/^{39}Ar age distribution pattern (Fig. 7b) wherein, to the NW of this boundary, biotite and amphibole ages range between 946 ± 2 and 885 ± 7 Ma (amphibole and biotite, respectively) and are systematically younger than ages in the Kongsberg LTU, which cluster between 1078 ± 1 to 995 ± 3 Ma (both biotite ages).

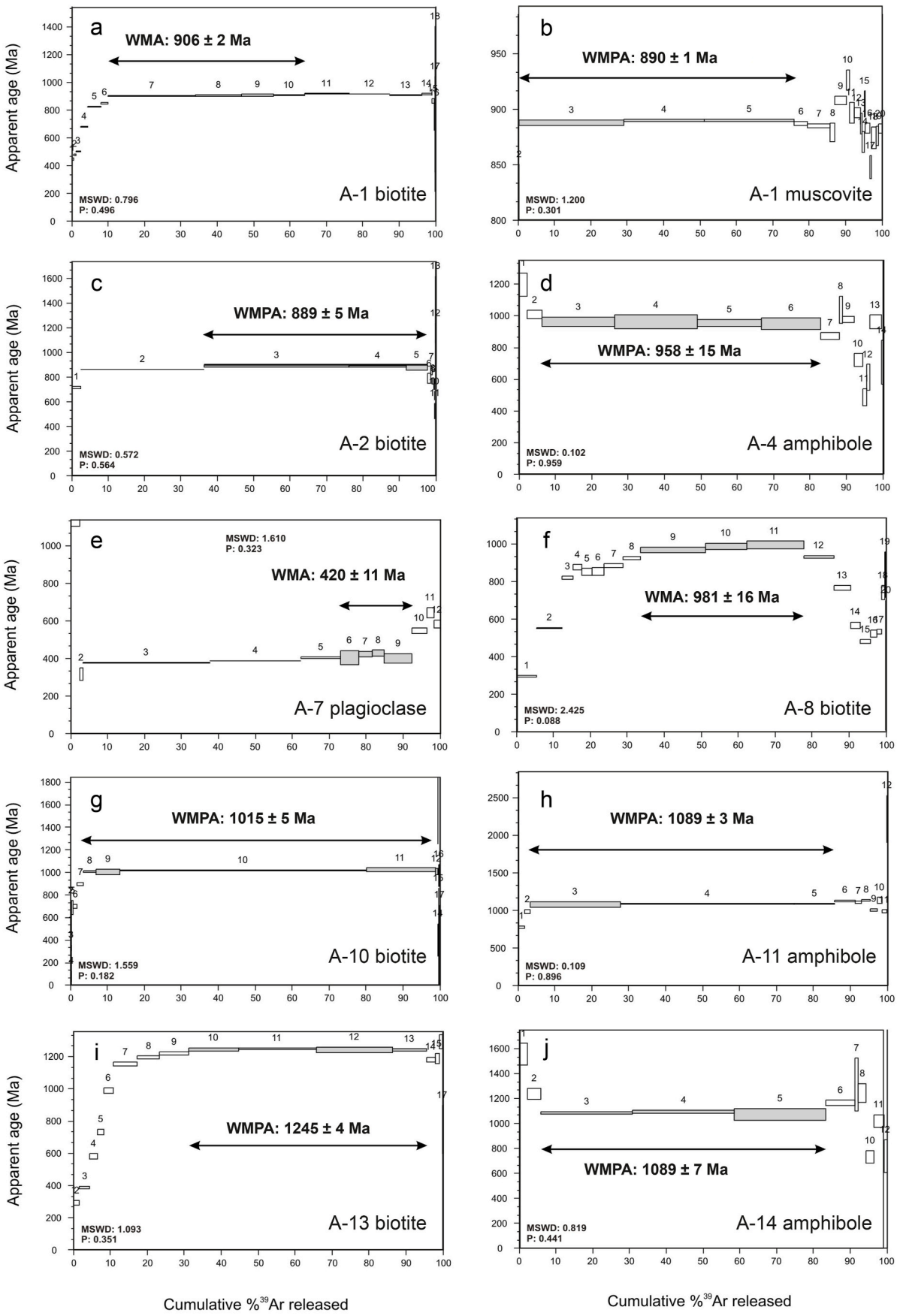

Fig. 3. $^{40}Ar/^{39}Ar$ degassing spectra (a-n, p) and one inverse isochron (o) of samples providing statistically robust dates from transect A-A′ (Fig. 2a).

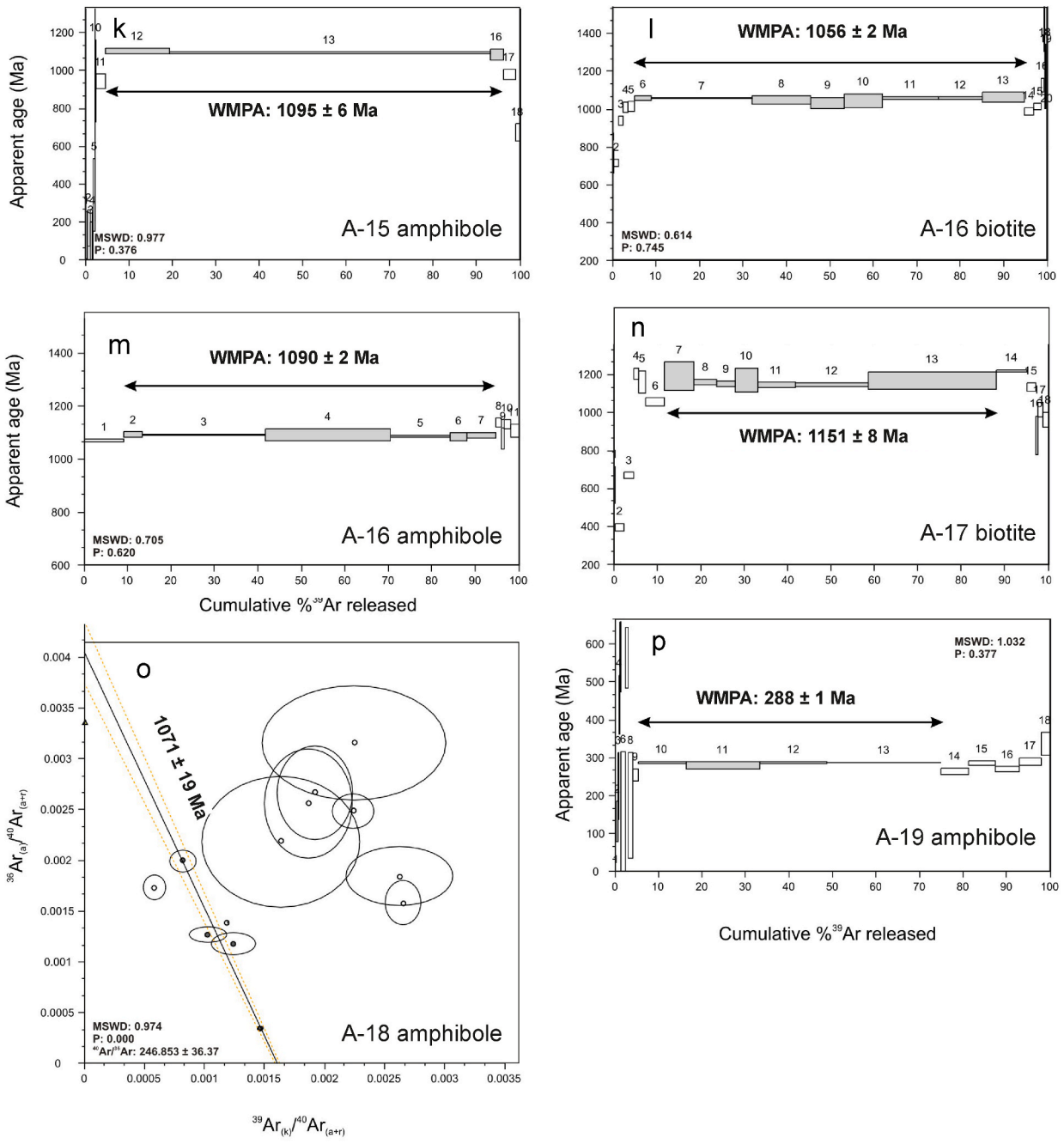

Fig. 3. (*continued*).

4.3. Transect C–C'

This transect crosses the northern part of the Kongsberg complex in the Kongsberg LTU into the Veme complex in the Idefjorden LTU (Figs. 2 and 7c), where the main gneissic foliation is affected by a complex fold pattern (Norefjell-Hønefoss fold; Scheiber et al., 2015). In the western part of the transect, ductile extensional structures occur, locally associated with partial melt pockets and migmatites (Fig. 6g). These include E-vergent folds at different scales and sets of localized steeply ESE-dipping normal faults affecting a broader zone. These faults are associated with pegmatitic dykes, especially where they deform competent mafic layers. In the narrow keel of the Kongsberg complex sandwiched between the granitic gneiss and the Modum complex, mylonitic rocks are abundant and are associated with sinistral shear kinematics (Fig. 6h). Structural relationships in the Kongsberg and Veme complex are complicated by a large-scale folding of the main foliation (Figs. 2b and 7c).

Eight $^{40}Ar/^{39}Ar$ step-heating ages were obtained from six samples from along this transect (Figs. 5 and 7c). The dated samples represent the gneisses of the Kongsberg complex, two are metasedimentary rocks of the Veme complex and one is from the Follum metadiorite in the eastern end of the transect (Fig. 2b), which has an intrusion age of c. 1555 Ma (Bingen et al., 2005). Except for a WMPA of 1079 ± 9 Ma from the Follum metadiorite sample (Fig. 5h), all the remaining data from this transect (one amphibole, two muscovite, five biotite) yield ages ranging from 1039 ± 55 to 971 ± 3 Ma. One WMPA (C1 biotite) is not taken into further consideration due to large analytical uncertainties (Fig. 5a).

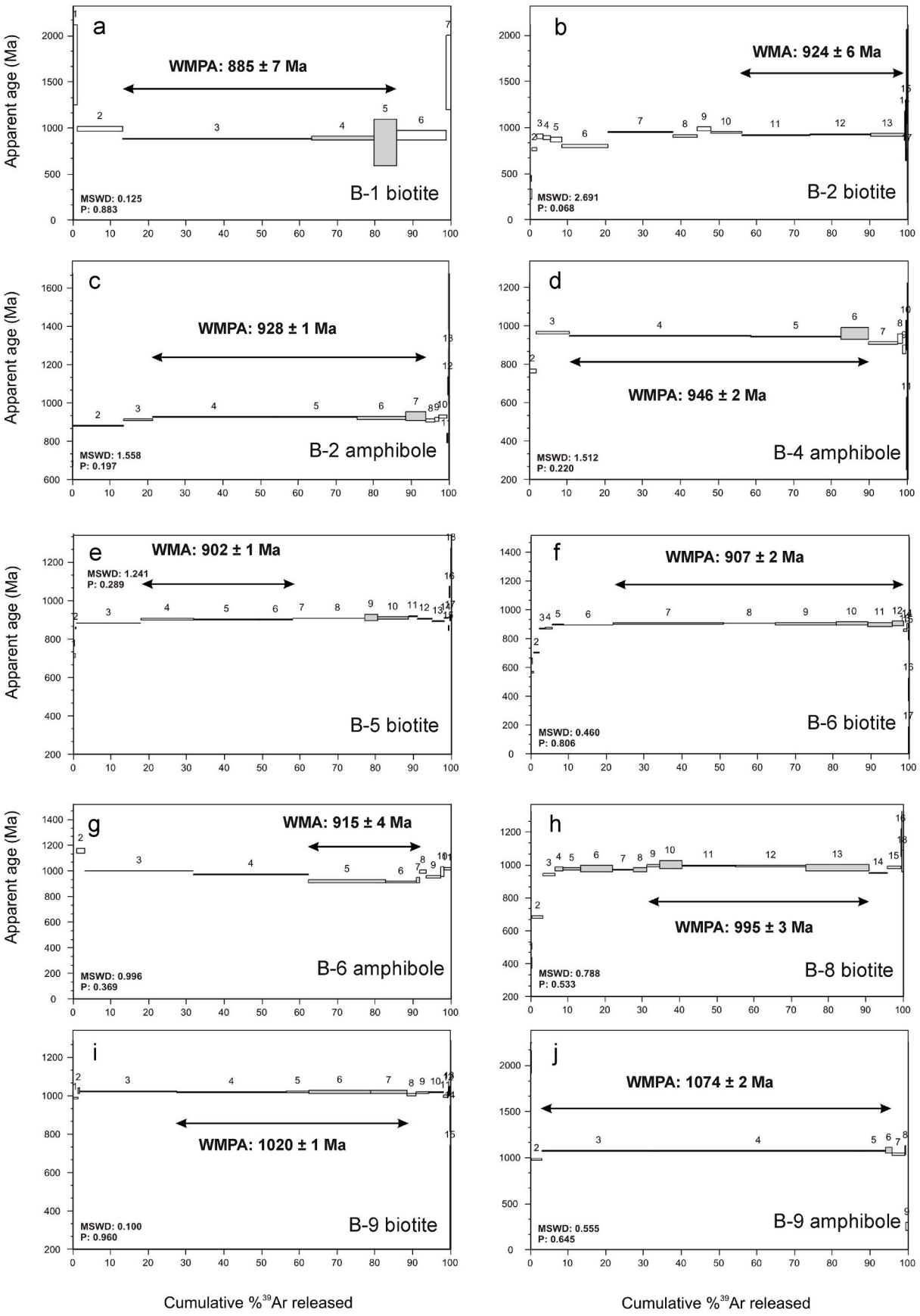

Fig. 4. $^{40}Ar/^{39}Ar$ degassing spectra of samples providing statistically robust dates from transect B–B′ (Fig. 2a).

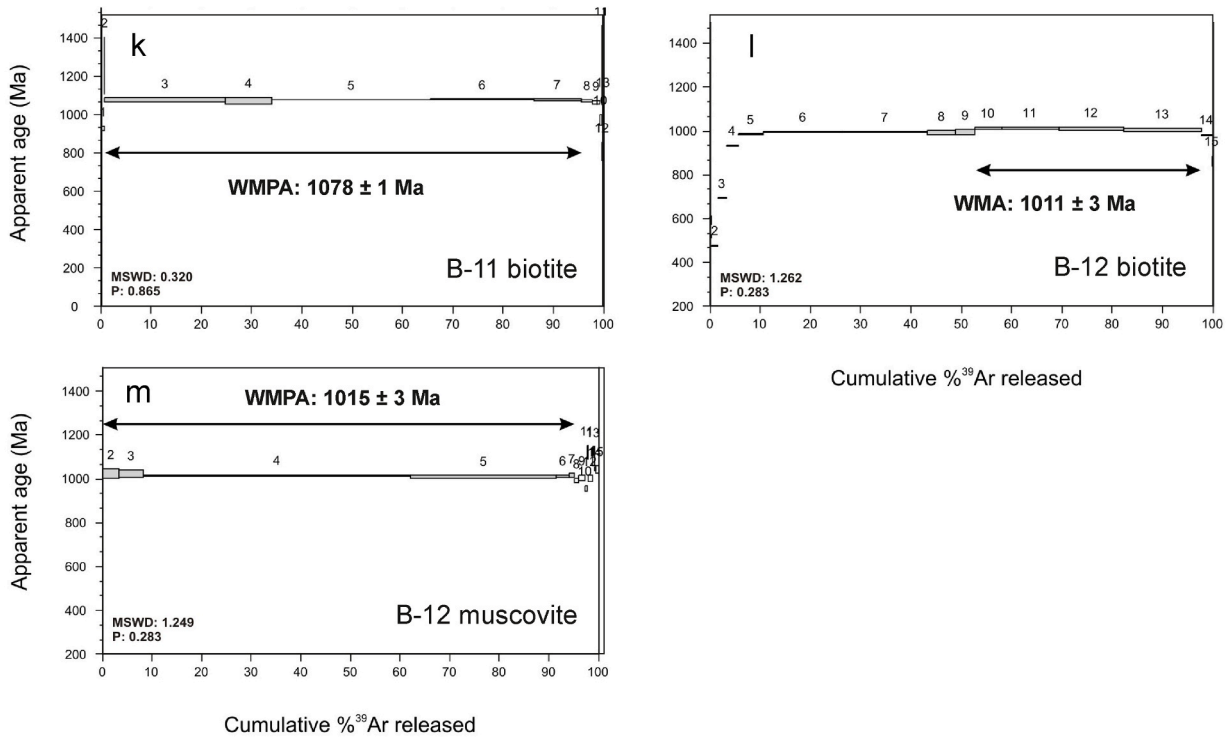

Fig. 4. (*continued*).

4.4. Microfabric of the dated samples

Microfabric analysis of sixteen representative dated samples shows that the dated minerals formed during different deformation processes according to their different structural settings as defined by the regional to macroscopic structural analysis (Figs. 2 and 7). As an example, a granitic gneiss sample (Fig. 8a) from the easternmost Telemark LTU is characterized by a granoblastic texture and the lack of a clear shape preferred mineral orientation. Biotite from this sample yields an $^{40}Ar/^{39}Ar$ age of 885 ± 7 Ma. Where a clear foliation is present (Fig. 8b), and especially where an E-plunging lineation is associated with the top-to-the-E shear fabric (Fig. 8c), the microfabric is characterized by recrystallization of amphibole, biotite, quartz, and feldspar and $^{40}Ar/^{39}Ar$ ages between c. 950 and 900 Ma. Large-scale subvertical sinistral shear zones deforming the Kongsberg LTU (Figs. 2 and 7) are microstructurally characterized by dynamically recrystallized quartz-rich aggregates hosting newly grown micas that are aligned along shear foliation planes (Fig. 8d). A detailed microstructural analysis of these shear zones is presented in Scheiber et al. (2015). Similarly, sheared rocks defining the Norefjell-Hønefoss fold pattern exhibit dynamic recrystallization and growth of both micas and amphiboles (Fig. 8e–f), indicating amphibolite facies conditions during shear deformation and folding. $^{40}Ar/^{39}Ar$ ages from such fabrics consistently spread around 1000 Ma. Finally, dated samples from the Kongsberg LTU are characterized by a weak shape-preferred mineral orientation and undulous extinction of quartz grains. Amphibole and micas largely lack signs of dynamic recrystallization (Fig. 8g–i) and yielded $^{40}Ar/^{39}Ar$ ages between c. 1060 and 1090 Ma.

4.5. The Prestfoss detachment

As a whole, the Kongsberg and Modum complexes are characterized by a steeply dipping amphibolite-to granulite-facies foliation which is folded into tight to isoclinal upright folds with shallowly plunging fold axes and variably plunging stretching lineations (Figs. 2 and 7). Subvertical mylonitic sinistral shear zones, formed under greenschist to amphibolite metamorphic conditions, deform the Kongsberg complex close to the KTBZ and adjacent to the Modum complex (Figs. 2 and 7). The dynamically recrystallized fabric of those shear zones is characterized by amphibole and mica defining the pervasive foliation (Fig. 8d–f) that overprints an older fabric (see also Scheiber et al., 2015).

Toward the west, however, the KTBZ is characterized by a very different structural framework, with a gently E-dipping to flat lying amphibolite-facies foliation. This abrupt change in structural architecture across the boundary between the Kongsberg complex and the KTBZ is notably associated with a change of the $^{40}Ar/^{39}Ar$ age pattern from older (c. 1100-1000 Ma) to significantly younger (c. 950-900 Ma) ages (Fig. 7). We interpret these structural, metamorphic, and geochronological changes as due to the presence of a newly discovered, and here geochronologically documented, regional-scale E-dipping extensional detachment zone, which we name the *Prestfoss detachment* (Fig. 9). Stretching lineations therein plunge to the E/ENE (Fig. 9a) and are invariably associated with top-to-the-E kinematic indicators (Figs. 6a, c, 6d, 6g, 9b-f). Structural measurements from the Prestfoss detachment are reported in the journal electronic repository (supplementary data). This detachment zone largely follows the contact between the Kongsberg LTU and the 1170-1145 Ma granitic gneiss (Figs. 2 and 7) and reactivated pre-existing mylonites and fault rocks (Scheiber et al., 2015). It caused footwall exhumation of the c. 1500 Ma biotite gneiss and of the 1170-1145 Ma granitic gneiss in the west. C. 950-900 Ma ago it juxtaposed these amphibolite-facies rocks against amphibolite-facies rocks of the Kongsberg complex, which had already cooled during the Sveconorwegian orogenic history between c. 1100-1000 Ma.

5. Time-constrained evolution of the central Sveconorwegian orogen

Our results demonstrate that the Kongsberg LTU and the KTBZ represent different structural domains, as also shown by their clearly different $^{40}Ar/^{39}Ar$ age signature. In the Kongsberg complex in the hanging wall of the Prestfoss detachment (Fig. 9a), the generally steeply dipping amphibolite facies foliation is associated with predominantly

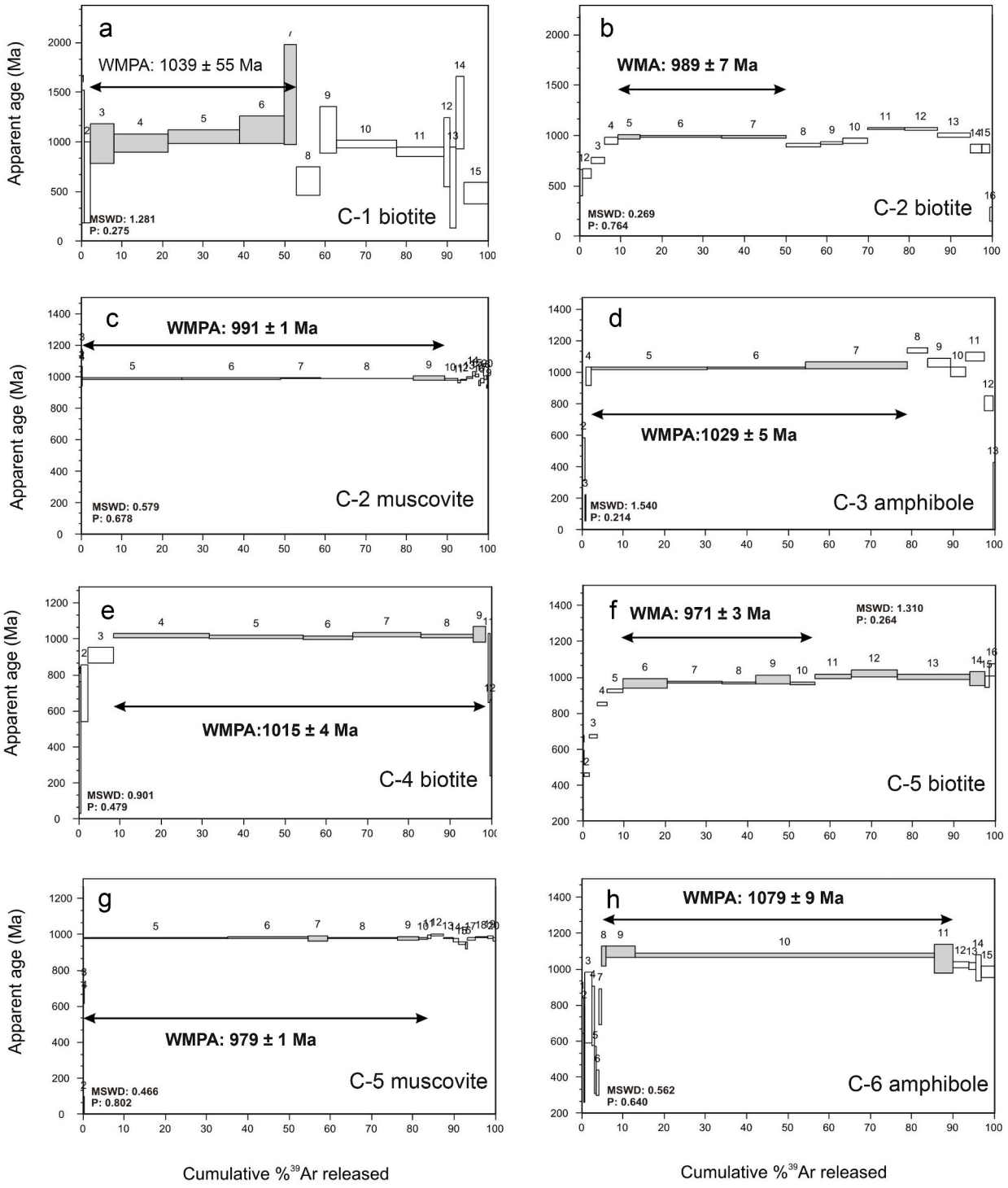

Fig. 5. $^{40}Ar/^{39}Ar$ degassing spectra of samples providing statistically robust dates from transect C–C′ (Fig. 2a).

Mesoproterozoic $^{40}Ar/^{39}Ar$ ages, while rocks in the footwall of the detachment (predominantly KTBZ rocks) are characterized by a gently-dipping to subhorizontal foliation and yield younger, predominantly Neoproterozoic $^{40}Ar/^{39}Ar$ ages (Figs. 7 and 10a-b). Here, we combine structural observations with the new $^{40}Ar/^{39}Ar$ ages to propose a deformation sequence for the study area. As to the detailed interpretation of the structural data, we build on the deformation history proposed by Scheiber et al. (2015).

5.1. Interpretation of $^{40}Ar/^{39}Ar$ dates

Individual $^{40}Ar/^{39}Ar$ dates can either be interpreted as dating (1) cooling to below a closure temperature below which radiogenic argon accumulates (McDougall and Harrison, 1999), (2) recrystallization of the dated mineral due to heat, strain or fluid circulation, which leads to resetting of the K–Ar system (Villa, 1998) or (3) a combination of the processes mentioned above resulting in mixed dates. Another quite common issue challenging the interpretation of $^{40}Ar/^{39}Ar$ data is given by the potential presence of “excess Ar”, i.e. ^{40}Ar in the dated mineral phase that is separated from its parent K (e.g., Kelley, 2002; Stübner

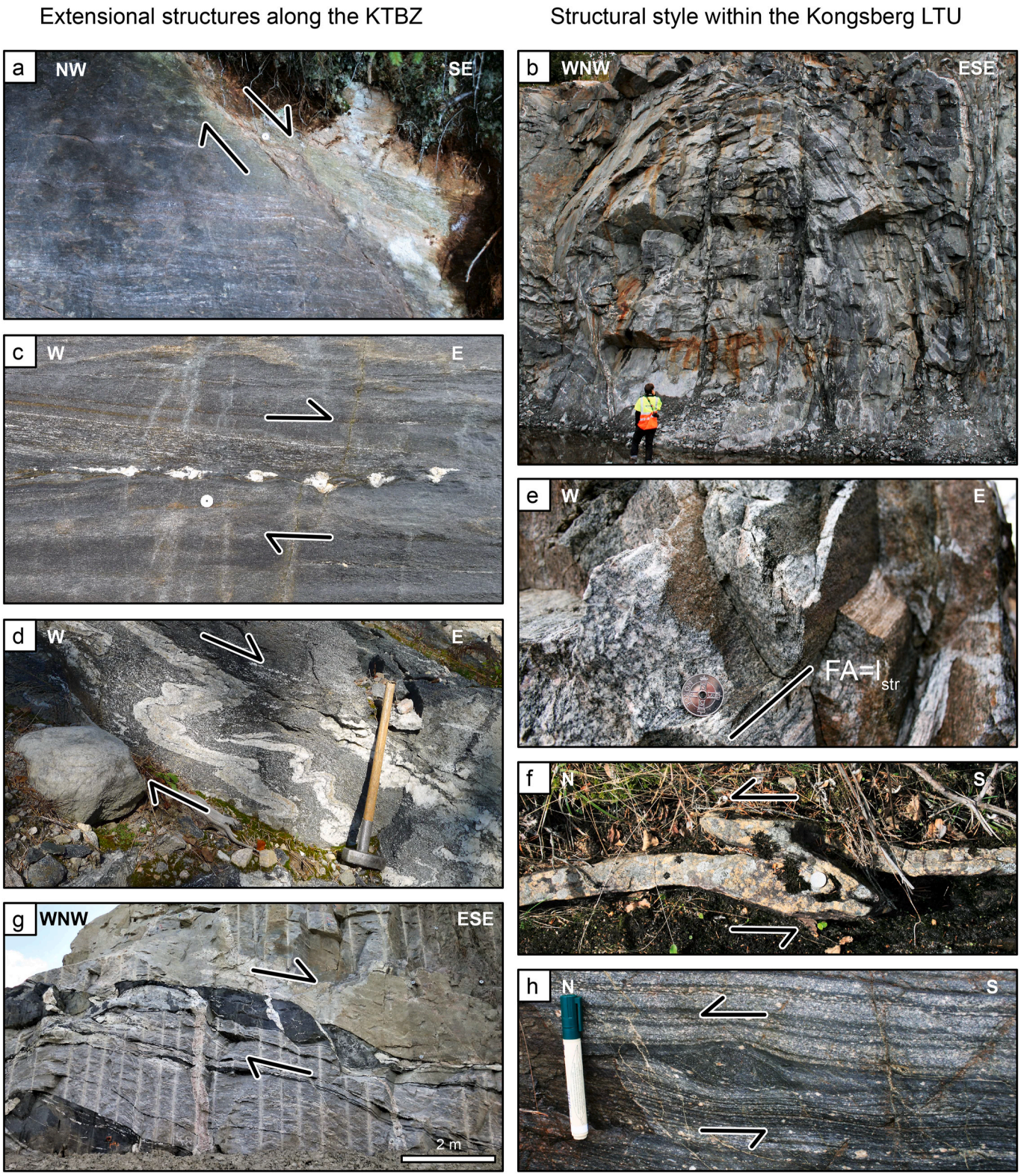

Fig. 6. Photographic plate showing structural characteristics from representative outcrops in the KTBZ (a, c, d, g) and from within the Kongsberg complex (b, e, f, h). (a) Discrete ductile to brittle C′-type shear band indicating top-to-the SE shearing (526618/6646416); coin for scale. (b) Upright isoclinal fold (532924/6626566); man for scale. Fold axis plunges gently towards the north. (c) Asymmetries of felsic boudins indicate top-to-the-SE sense of shear (523119/6641628); coin for scale. (d) East-vergent folds (539960/6669946); hammer for scale. (e) Isoclinal upright fold (538090/6659814); coin for scale. Fold axis (FA) is parallel to the sub-horizontal stretching lineation (lstr). (f) Top view of folded competent felsic layer (540912/6648122) indicating sinistral shear deformation; coin for scale. (g) Roadcut (543264/6681689) revealing asymmetric boudinage of mafic layers in strongly foliated granitic gneiss indicating top-to-the-SE shearing. Boudinage is associated with pegmatitic dyke intrusion. (h) Top view of lithologically heterogeneous mylonitic package dipping moderately to the E (546056/6673446); marker pen for scale. Asymmetric mafic lens indicates sinistral shearing. Localities of the outcrops are shown in Fig. 7.

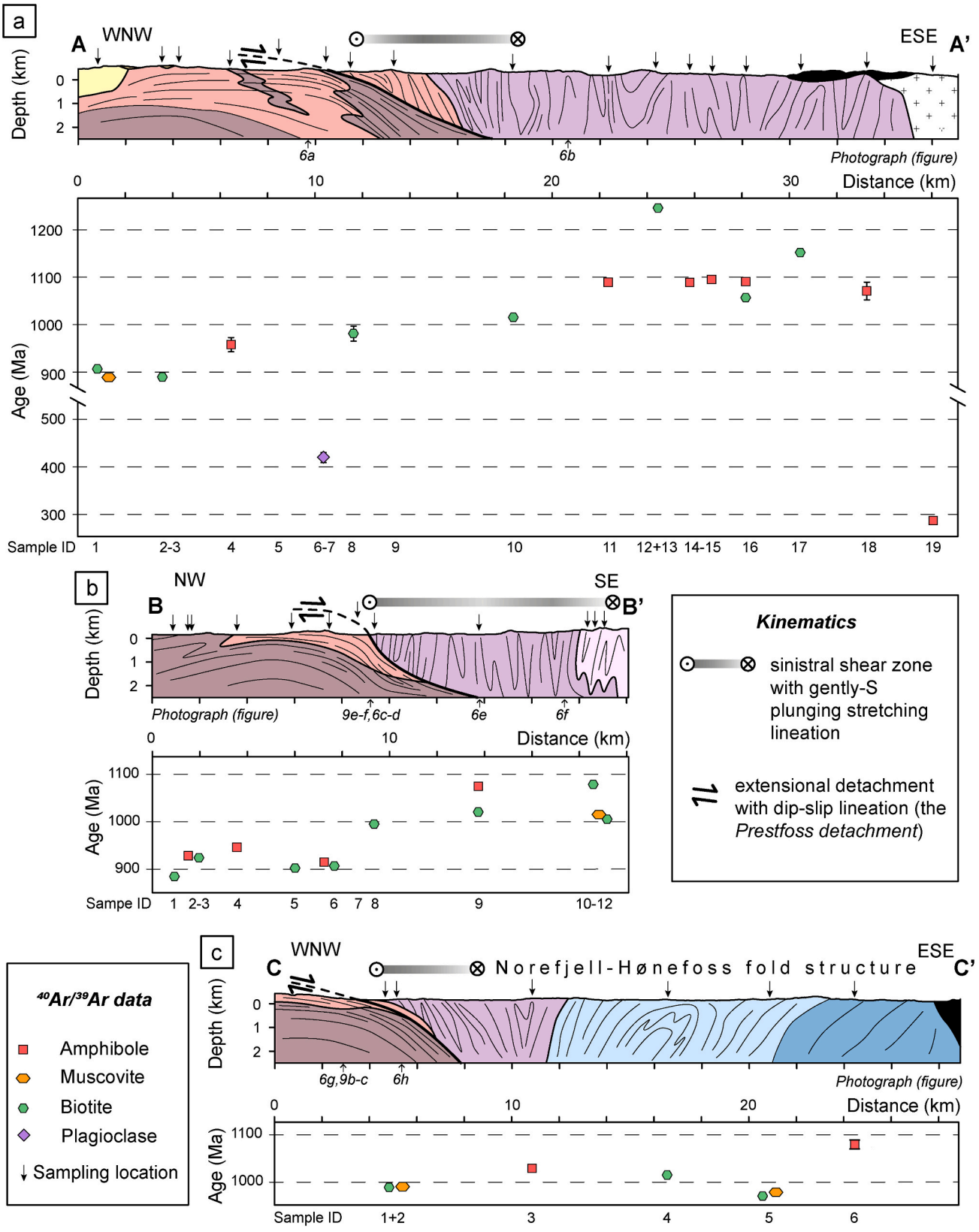

Fig. 7. Geological cross sections and corresponding $^{40}Ar/^{39}Ar$ data from three sampled transects. Cross sections: Geological units are color-coded according to the map of Fig. 2a. Subvertical sinistral shear zones (increasing shear intensity with increasing gray-value) and extensional top-to-the-E shear zones are highlighted. Projected locations of photographs presented in Fig. 6 and 9 are provided. (For interpretation of the references to color in this figure legend, the reader is referred to the Web version of this article.)

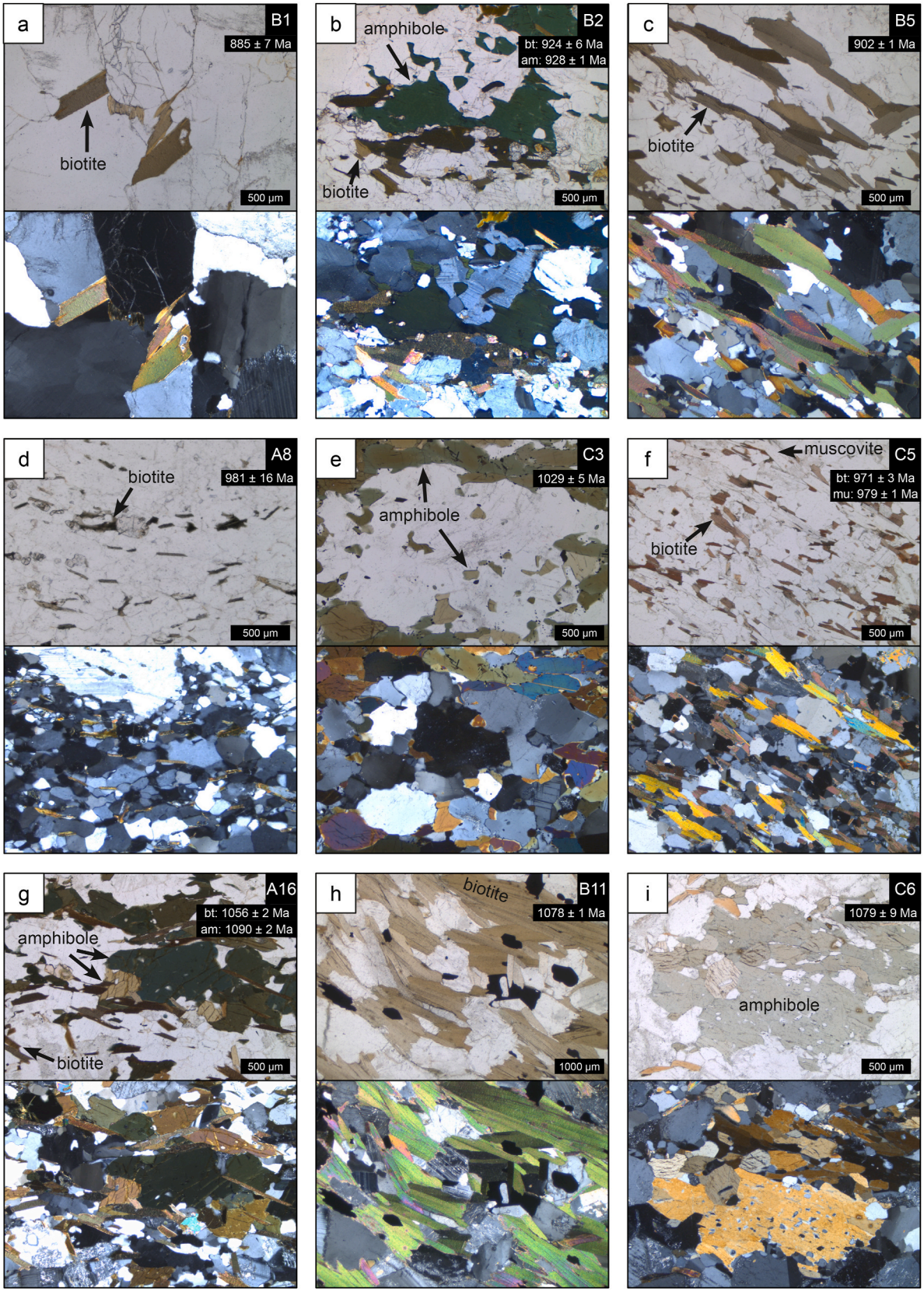

Fig. 8. Summary plate of plane-polarized (above) and cross-polarized light micrographs (below) of representative fabrics from (a–c) the easternmost Telemark LTU including (c) the Prestfoss detachment, (d) a sinistral shear zone hosted by the KTBZ, (e–f) the Norefjell-Hønefoss fold structure, and from (g–h) the Kongsberg and Modum complexes. Sample ID and $^{40}Ar/^{39}Ar$ ages (see Figs. 2a and 7 for sample localities) are provided in the upper right corner (am = amphibole, bt = biotite, mu = muscovite). Sample C6 is from the Follum metadiorite (Fig. 2a).

et al., 2017), which makes the mineral date apparently older. Excess ^{40}Ar can be an issue particularly when dealing with cooling histories of geologically old rocks, because of the potential for accumulation of ^{40}Ar (which causes excess Ar) within grain boundary networks (Kelley, 2002).

In order to address the problem of excess argon in our samples, we investigated all step-heating results by relying on ^{38}Ar (supplementary data) and ^{37}Ar (step heating diagrams, supplementary data) as proxies

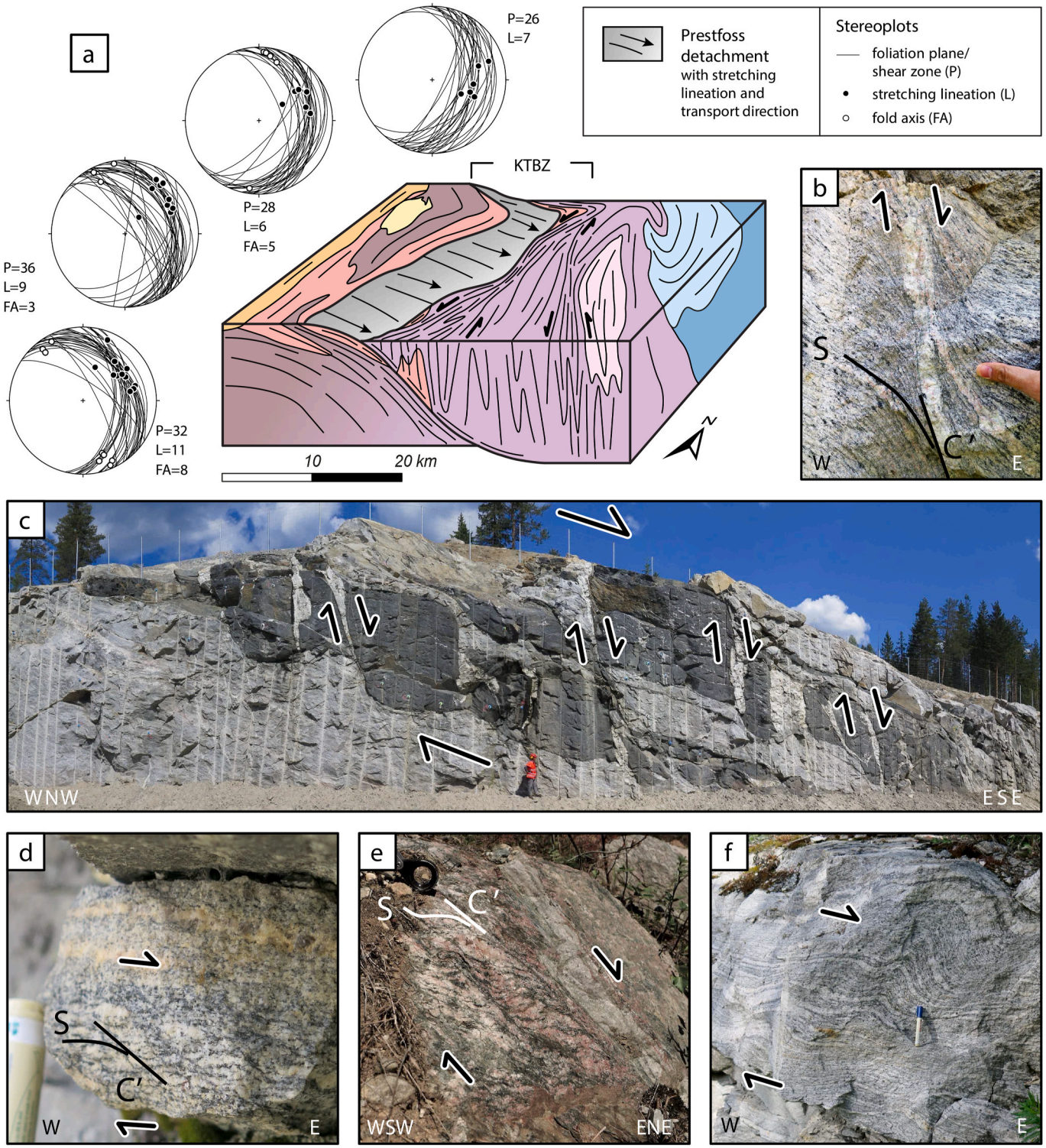

Fig. 9. (a) Lower-hemisphere and equal-area projection of structural data (cf. supplementary data) from the Prestfoss detachment and schematic block diagram illustrating exhumation along the detachment. (b–f) Field aspects from the Prestfoss detachment. (b) Ductile C′-type top-to-the-E shear band affecting the granitic gneiss is associated with melting (543264/6681689); finger for scale. This photograph has been mirrored in order to present all photographs in the same orientation. (c) Road cut (543422/6681585) exposing asymmetric boudinage of mafic layers and melt injection along extensional shear zones; man for scale. (d–e) S–C′ fabrics (531960/6657151, marker pen for scale; and 536195/6662534, magnifier for scale) indicating top-to-the-E(NE) transport. (f) Asymmetric E-vergent open folding (529408/6660266); marker pen for scale. Localities of the outcrops are shown in Fig. 7.

for contaminant Ca phases and sources of excess ^{40}Ar from Cl-rich fluid inclusions. We found no correlation between age and $^{37}Ar_{Ca}/^{39}Ar_k$ ratios, and we therefore conclude that the applied interference corrections satisfactorily have corrected for the contaminant. For the step-heating experiments forming age plateaus, we find no correlation between age and variation with $^{38}Ar/^{39}Ar_k$. In some cases, however, there are old apparent ages at higher temperature steps, which correlate with high $^{38}Ar/^{39}Ar_k$ ratios, consistent with breaching of the crystalline lattice where excess ^{40}Ar is released.

Distinguishing between cooling and recrystallization ages can be challenging as well. If the $^{40}Ar/^{39}Ar$ ages of the various minerals are significantly different and become younger with commonly reported lower closure temperatures (Schaen et al., 2020), they likely result from (relatively slow) cooling. This is, however, based on the assumption that the K–Ar system is not significantly affected by diffusion processes after the dated sample has crossed the relevant closure temperature, which is particularly problematic in slowly cooled plutonic or metamorphic rocks in the middle and lower crust and in multiply deformed terranes en route to the surface (e.g., Kelley, 2002; McDougall and Harrison, 1999; Schaen et al., 2020; Villa, 1998; Warren et al., 2012). If $^{40}Ar/^{39}Ar$ ages from different mineral phases from one sample or from one structural domain are statistically identical, they either indicate very rapid cooling to below the closure temperatures of the dated phases (e.g., Yang et al., 2007) or later deformation and recrystallization (e.g., Scheiber et al., 2016). These two scenarios may be discriminated by investigating the microfabric of the dated samples and the chemical composition of the dated minerals.

In our study, $^{40}Ar/^{39}Ar$ ages obtained from different mineral phases from the same sample largely correspond to the cooling sequence expected from the known closure temperatures for the different dated mineral phases (Schaen et al., 2020) (cf. Table 2, Figs. 3–5, 7): amphibole ages are, thus, systematically older than biotite ages from the same samples (A-16, B-2, B-6, B-9), and are, together with their microstructural setting, therefore generally interpreted to represent cooling ages. Muscovite ages on the other hand, are generally slightly older or identical within error to biotite ages from the same samples (B-12, C-2, C-5) indicating very rapid cooling or recrystallization of both mica minerals, or, alternatively, excess Ar affecting biotite. The Kernel density estimates of our ages (Fig. 10a–b) reveal a pattern of muscovite peaks overlapping with and tending to be slightly younger than biotite peaks. Although our dataset includes only three muscovite ages, this pattern is similar to what has been observed in a large compilation of Precambrian $^{40}Ar/^{39}Ar$ data from the northern Canadian Shield, where the relatively old biotites are explained by excess argon (Kellett et al., 2020).

There occur two unexpectedly old biotite ages in our dataset. The 1245 ± 4 Ma age (A-13, Fig. 3i) clearly predates the Sveconorwegian evolution, and the 1151 ± 8 Ma age (A-17, Fig. 3n) slightly predates Sveconorwegian peak metamorphism constrained with zircon U–Pb data to c. 1145 to 1130 Ma (Bingen and Viola, 2018). While the reason for the old age of gneiss sample A-17 remains unknown, sample A-13 is from a phyllonite overprinting the Sveconorwegian fabric and its apparent old age can possibly be related to ^{40}Ar release during post-Sveconorwegian deformation. We point out that even though the $^{40}Ar/^{36}Ar$ intercepts of these samples overlap with the modern air composition (Lee et al., 2006), excess Ar can still be present but hidden in the large $^{40}Ar/^{36}Ar$ intercept uncertainties caused by the high radiogenic Ar component of these minerals. Planar defects have also been suggested to cause elevated Ar retentivity in trioctahedral micas (Camacho et al., 2012). Based on these two old ages notwithstanding, the age patterns documented by our dataset and their spatial and genetic relationship with specific structural domains (Figs. 7 and 10) allow for a confident interpretation of the Meso- and Neoproterozoic, Paleozoic (Silurian) and Mesozoic (Permian) ages as follows.

5.2. Early Sveconorwegian (Mesoproterozoic) cooling

In the Kongsberg LTU, six $^{40}Ar/^{39}Ar$ amphibole ages cluster at c. 1090 Ma, two biotite ages cluster at c. 1070 Ma and eight biotite ages at c. 1000 Ma (Fig. 10a). These ages postdate the regional peak amphibolite-to granulite-facies metamorphism in the Kongsberg LTU constrained by U–Pb zircon geochronology to between 1145 and 1130 Ma (Bingen and Viola, 2018), with later metamorphic mineral growth documented down to c. 1080 Ma (cf. Table 1; Andersen and Grorud, 1998; Bingen et al., 2001; Bingen et al., 2008a; Munz et al., 1994). The c.1090 Ma amphibole and the subtle 1070 Ma biotite peaks in the Kernel distributions of our dataset (Fig. 10a) are interpreted as the most representative ages constraining cooling following regional-scale, early Sveconorwegian deformation and metamorphism (Fig. 10). Such ages are particularly common in the southernmost transect A-A′ but are also present in the areas sampled along transects B–B′ and C–C' (Fig. 7). The 1079 ± 9 Ma amphibole age from transect C–C' is from the Follum metadiorite (Fig. 2b), which represents a relatively competent body compared to the adjacent Veme and Kongsberg complexes, and which, therefore, largely escaped significant later Sveconorwegian deformation. Evidence of early Sveconorwegian deformation and high-grade metamorphism has also been reported from the Bamble LTU (Fig. 1; Bingen and Viola, 2018; Engvik et al., 2016; Nijland et al., 2014), where metasomatic processes dated to between c. 1100 and 1080 Ma (Engvik et al., 2017) and reported hornblende cooling ages of 1090–1080 Ma (Cosca et al., 1998) overlap with our $^{40}Ar/^{39}Ar$ amphibole ages from the Kongsberg LTU (Fig. 10). Hence, our data confirm that the Kongsberg and Bamble LTUs underwent the same early Sveconorwegian evolution (cf. Bingen et al., 2021).

5.3. Sveconorwegian (Meso-to Neoproterozoic) sinistral transpression and large-scale folding in the Kongsberg LTU

Large-scale sinistral shearing affected the Kongsberg complex and, in the southern part of the study area, also the granitic gneiss of the KTBZ (Figs. 2b, 7 and 9a). Subhorizontal to gently S-plunging stretching lineations along subvertical c. N–S trending mylonitic shear zones are associated with pervasive amphibolite-to greenschist-facies sinistral shear kinematics (Fig. 6f and h) and formed as a result of sinistral transpression (Scheiber et al., 2015). Two $^{40}Ar/^{39}Ar$ muscovite and six biotite ages from these shear zones are similar and generally cluster at around 1000 Ma (Fig. 10). In addition, one similar muscovite and two biotite ages occur in the area deformed by the Norefjell-Hønefoss fold structure including the Kongsberg and the Veme complexes (Figs. 2b and 7). In the Kernel distributions of the ages obtained from the hanging wall of the Prestfoss detachment (Fig. 10a), the broad $^{40}Ar/^{39}Ar$ biotite peak age at c. 1000 Ma overlaps with $^{40}Ar/^{39}Ar$ muscovite ages. This age pattern is interpreted as reflecting resetting of both minerals by deformation and recrystallization (Fig. 8d–f) along sinistral shear zones overprinting an older fabric. The documented spatial distribution of $^{40}Ar/^{39}Ar$ ages indicates that large-scale folding in the Norefjell-Hønefoss area is genetically and temporally linked to sinistral shear deformation in the Kongsberg LTU. The generally gently S-plunging stretching lineation associated with the shear zones indicates that shearing led to the overall uplift of the eastern block(s) relative to the western block(s). The amphiboles were, however, not or just little affected by this deformation event (Fig. 7c; cf. sample C-3). Also, some biotites from the Modum complex (cf. sample B11) escaped resetting of the K–Ar system, which indicates that deformation had localized along discrete shear zones within a larger area affected by overall sinistral transpression.

Our new $^{40}Ar/^{39}Ar$ muscovite and biotite ages constraining sinistral shear deformation overlap with the 1012 ± 7 to 985 ± 5 Ma metamorphic U–Pb zircon and titanite ages (Bingen et al., 2008a) from the Vardefjell shear zone (Table 1), which represents the northwestern continuation of the sinistral shear zones in the Kongsberg LTU (Figs. 1b

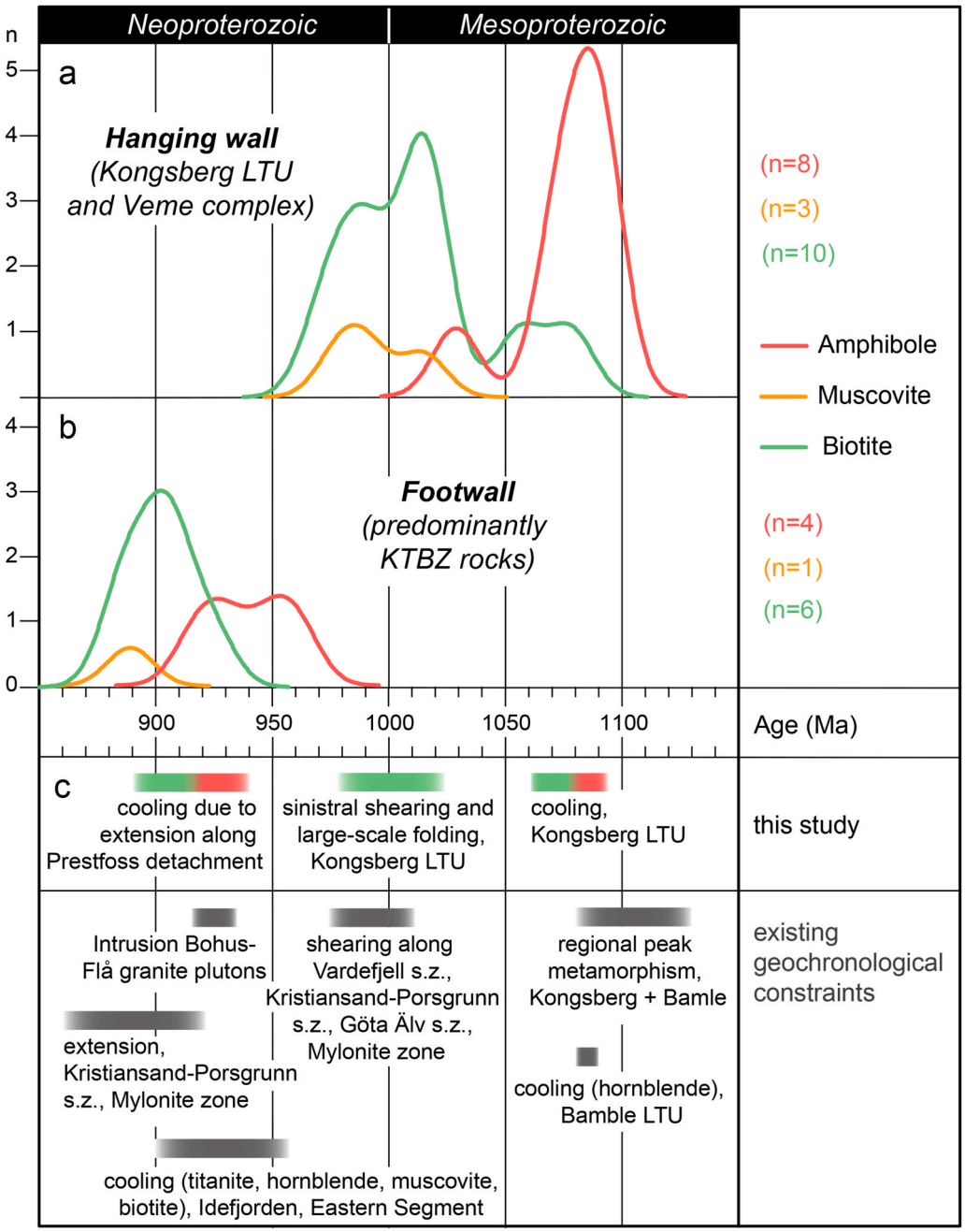

Fig. 10. Kernel density estimates of the Sveconorwegian $^{40}Ar/^{39}Ar$ ages from (a) the hanging wall and the (b) footwall of the Prestfoss detachment. Bandwith = 10 Ma. (c) Interpretation of the Sveconorwegian $^{40}Ar/^{39}Ar$ ages and correlation with published geochronological data (see text for further explanation).

and 2a). These sinistral shear zones form part of a larger c. N–S trending transpressive shear belt documented in the Sveconorwegian orogen of S Norway and SW Sweden (Bergström et al., 2020; Hageskov, 1980, 1985; Stephens et al., 1996). Top-to-the-NW deformation along the Kristiansand-Porsgrunn shear zone (Fig. 1b) has been dated to 994 ± 30 Ma (titanite; de Haas et al., 2002). The Göta Älv shear zone deforming the Ideforden LTU (Fig. 1b) is interpreted as a sinistral strike-slip zone (Park et al., 1991) dated to 974 ± 22 Ma (zircon; Ahlin et al., 2006), and metamorphic zircons constraining sinistral transpression along the Mylonite Zone (Viola et al., 2011) yield 980 ± 13 Ma (Andersson et al., 2002) and 971 ± 8 Ma ages (Larson et al., 1999).

5.4. Late Sveconorwegian (Neoproterozoic) detachment faulting

The $^{40}Ar/^{39}Ar$ ages obtained from the KTBZ (that is, from within the footwall block) are significantly younger than those from the Kongsberg LTU in the hanging wall of the Prestfoss detachment, with an amphibole age distribution at c. 940 Ma, a biotite peak at c. 900 Ma and one muscovite age of c. 890 Ma (Fig. 10b). Our new $^{40}Ar/^{39}Ar$ data thus constrain extension along the Prestfoss detachment and cooling of the footwall due to exhumation of KTBZ rocks and lower levels of the Kongsberg LTU (Fig. 9). The local occurrence of migmatites and melt pockets in the immediate footwall (Figs. 6 and 9) as well as the gradual decrease of metamorphic grade towards the Telemark supracrustal successions in the west suggest that E-directed shearing along the Prestfoss detachment led to the formation of an immature asymmetric core complex (as similarly reported from the Eastern Segment by Viola et al., 2011). Extensional shearing along the Prestfoss detachment started prior to the 930 Ma intrusion (U–Pb zircon ages) of the Flå granite (Bingen et al., 2008b; Lamminen et al., 2011), which is part of the 930-915 Ma

Bohus-Flå granite belt (U–Pb zircon ages; Andersson et al., 1996; Eliasson and Schöberg, 1991). The fact that both biotite and muscovite $^{40}Ar/^{39}Ar$ ages are similar (Figs. 7 and 10b) may indicate a thermal event resetting both mica ages, such as the intrusion of large igneous bodies. Thermal resetting of the $^{40}Ar/^{39}Ar$ mica ages in our transects due to large intrusions is, however, unlikely due to the large (several tens of km) distance between the Flå granite and the sampling localities west of the Prestfoss detachment (Fig. 2a).

Extensional deformation along pre-existing fabrics has also been reported from other major shear zones in the Sveconorwegian orogen. These include the Kristiansand-Porsgrunn shear zone, the Mylonite zone and the Sveconorwegian frontal deformation zone (SFDZ). Muscovite and biotite $^{40}Ar/^{39}Ar$ data from these shear zones constrain extensional deformation to between c. 930 and 860 Ma (Mulch et al., 2005; Viola et al., 2011), and U–Pb titanite and amphibole, muscovite and biotite $^{40}Ar/^{39}Ar$ data document associated regional cooling (Connelly et al., 1996; Page et al., 1996a, 1996b; Ulmius et al., 2018; Wang et al., 1998). Late-Sveconorwegian extensional deformation and cooling is generally interpreted to reflect the end of convergence in the orogen and associated collapse of the orogenic edifice (Bingen et al., 2006, 2021).

6. Post-Sveconorwegian Paleozoic ages from the Kongsberg LTU and the Oslo Rift

$^{40}Ar/^{39}Ar$ analysis of plagioclase yields a Paleozoic, late Silurian (420 ± 11 Ma) age (Figs. 3e and 7a). This age coincides in time with the well-known tectonic phase of Caledonian SE-directed nappe emplacement (Dunlap and Fossen, 1998). Although no Caledonian rocks are preserved in the study area (Fig. 1), the Caledonian orogenic edifice covered most probably also the Sveconorwegian rocks of the Telemark and Kongsberg LTUs, and the obtained early Paleozoic age may therefore be interpreted as (partial) resetting of the K–Ar system in the plagioclase due to Caledonian tectonics.

The Permian $^{40}Ar/^{39}Ar$ amphibole age of 288 ± 1 Ma from the Oslo Rift (Fig. 3p) dates the intrusion of the alkali-feldspar granite (ekerite) pluton along the shores of the Eikeren lake (Pedersen et al., 1995). This age overlaps with the extrusion of rhomb porphyry volcanic sequences (Krokskogen area, 300–280 Ma, Corfu and Larsen, 2020) and is in the age range of the oldest known plutons in the Oslo Rift (Larvik plutonic complex, 298–292 Ma, Dahlgren et al., 1996).

7. Conclusions

The results of this study allow reassessment of the timing of the main deformation and exhumation events in the Kongsberg LTU and adjacent LTUs of the Sveconorwegian orogen of southern Norway:

(1) Cooling of the Kongsberg LTU to below biotite closure temperature between c. 1090 and 1070 Ma is compatible with early Sveconorwegian regional amphibolite to granulite facies deformation documented in the Kongsberg and Bamble LTUs.
(2) Sinistral shearing at around 1000 Ma along the KTBZ and along shear zones within the Kongsberg LTU led to local large-scale folding of the pre-existing early-Sveconorwegian foliation. These deformation structures formed as a result of transpression accommodated by a number of c. N–S trending shear zones in the Sveconorwegian orogen of S Norway and SW Sweden.
(3) Late-Sveconorwegian extensional shearing along the Prestfoss detachment between c. 940 and 900 Ma caused the exhumation of amphibolite facies gneiss and quartzite of the Telemark LTU and their juxtaposition against amphibolite facies gneisses of the Kongsberg LTU and the KTBZ, which had already cooled earlier during the Sveconorwegian orogeny. Extensional shearing along the Prestfoss detachment began prior to the emplacement of the Flå granite in the hanging wall of the detachment at c. 930 Ma. The Prestfoss detachment led to the formation of an immature asymmetric core complex, which is in agreement with overall gradually decreasing metamorphic grade towards the Telemark supracrustal successions to the west.

CRediT author statement

Thomas Scheiber: Investigation, Formal Analysis (structural data), Writing – Original Draft, Visualization.

Giulio Viola: Conceptualization, Supervision, Project administration, Investigation, Writing – Review & Editing.

Morgan Ganerød: Formal Analysis (Ar–Ar data), Writing – Review & Editing.

Bernard Bingen: Investigation, Writing – Review & Editing.

Declaration of competing interest

The authors declare that they have no known competing financial interests or personal relationships that could have appeared to influence the work reported in this paper.

Data availability

The authors do not have permission to share data.

Acknowledgments

This paper presents some of the results obtained during the KONGMO project hosted and initiated by the Geological Survey of Norway and partly financially supported by the former Telemark, Vestfold and Buskerud counties. We thank Camilla Maya Wilkinson for assistance in the Ar/Ar laboratory. Constructive comments by Stanislaw Mazur and by two anonymous reviewers improved the manuscript. Toru Takeshita is thanked for careful editorial handling.

Supplementary data

Supplementary data to this article can be found online at https://doi.org/10.1016/j.jsg.2022.104777.

References

Ahlin, S., Hegardt, E.A., Cornell, D., 2006. Nature and stratigraphic position of the 1614 Ma Delsjön augen granite-gneiss in the Median Segment of south-west Sweden. GFF 128, 21–32.
Anczkiewicz, R., Viola, G., Müntener, O., Thirlwall, M.F., Villa, I.M., Quong, N.Q., 2007. Structure and shearing conditions in the day Nui Con Voi massif: implications for the evolution of the red river shear zone in northern Vietnam. Tectonics 26.
Andersen, T., Andresen, A., Sylvester, A.G., 2002. Timing of late-to post-tectonic Sveconorwegian granitic magmatism in South Norway. Geol. Surv. Norway Bull. 440, 5–18.
Andersen, T., Griffin, W.L., Jackson, S.E., Knudsen, T.L., Pearson, N.J., 2004. Mid-Proterozoic magmatic arc evolution at the southwest margin of the Baltic Shield. Lithos 73, 289–318.
Andersen, T., Grorud, H.-F., 1998. Age and lead isotope systematics of uranium-enriched cobalt mineralization in the Modum complex, South Norway: implications for Precambrian crustal evolution in the SW part of the Baltic Shield. Precambrian Res. 91, 419–432.
Andersen, T., Munz, I.A., 1995. Radiogenic whole-rock lead tn Precambrian metasedimentary gneisses from South Norway: evidence of Sveconorwegian LILE mobility. Norw. J. Geol. 75, 156–168.
Andersson, J., Möller, C., Johansson, L., 2002. Zircon geochronology of migmatite gneisses along the Mylonite Zone (S Sweden): a major Sveconorwegian terrane boundary in the Baltic Shield. Precambrian Res. 114, 121–147.
Andersson, M., Lie, J.E., Husebye, E.S., 1996. Tectonic setting of post-orogenic granites within SW Fennoscandia based on deep seismic and gravity data. Terra. Nova 8, 558–566.
Austrheim, H., Putnis, C.V., Engvik, A.K., Putnis, A., 2008. Zircon coronas around Fe–Ti oxides: a physical reference frame for metamorphic and metasomatic reactions. Contrib. Mineral. Petrol. 156, 517–527.
Bergström, U., Stephens, M.B., Wahlgren, C.-H., 2020. Chapter 16 Polyphase (1.6–1.5 and 1.1–1.0 Ga) deformation and metamorphism of Proterozoic (1.7–1.1 Ga) continental crust, Idefjorden terrane, Sveconorwegian orogen. Geol. Soc. London, Memoirs 50, 397–434.

Bingen, B., Birkeland, A., Nordgulen, Ø., Sigmond, E.M.O., 2001. Correlation of supracrustal sequences and origin of terranes in the Sveconorwegian orogen of SW Scandinavia: SIMS data on zircon in clastic metasediments. Precambrian Res. 108, 293–318.
Bingen, B., Davis, W.J., Hamilton, M.A., Engvik, A.K., Stein, J.J., Skår, Ø., Nordgulen, Ø., 2008a. Geochronology of high-grade metamorphism in the Sveconorwegian belt, S. Norway: U-Pb, Th-Pb and Re-Os data. Norw. J. Geol. 88, 13–42.
Bingen, B., Nordgulen, Ø., Sigmond, E.M.O., Tucker, R., Mansfeld, J., Högdahl, K., 2003. Relations between 1.19–1.13 Ga continental magmatism, sedimentation and metamorphism, Sveconorwegian province, S Norway. Precambrian Res. 124, 215–241.
Bingen, B., Nordgulen, Ø., Viola, G., 2008b. A four-phase model for the Sveconorwegian orogeny, SW Scandinavia. Norw. J. Geol. 88, 43–72.
Bingen, B., Skår, Ø., Marker, M., Sigmond, E.M.O., Nordgulen, Ø., Ragnhildstveit, J., Mansfeld, J., Tucker, R.D., Liégeois, J.-P., 2005. Timing of continental building in the Sveconorwegian orogen, SW Scandinavia. Norw. J. Geol. 85, 87–116.
Bingen, B., Stein, H.J., Bogaerts, M., Bolle, O., Mansfeld, J., 2006. Molybdenite Re–Os dating constrains gravitational collapse of the Sveconorwegian orogen, SW Scandinavia. Lithos 87, 328–346.
Bingen, B., Viola, G., 2018. The early-Sveconorwegian orogeny in southern Norway: tectonic model involving delamination of the sub-continental lithospheric mantle. Precambrian Res. 313, 170–204.
Bingen, B., Viola, G., Möller, C., Vander Auwera, J., Laurent, A., Yi, K., 2021. The Sveconorwegian orogeny. Gondwana Res. 90, 273–313.
Blereau, E., Johnson, T.E., Clark, C., Taylor, R.J.M., Kinny, P.D., Hand, M., 2017. Reappraising the P–T evolution of the Rogaland–Vest Agder sector, southwestern Norway. Geosci. Front. 8, 1–14.
Bodorkos, S., Clark, D.J., 2004. Evolution of a crustal-scale transpressive shear zone in the Albany–Fraser Orogen, SW Australia: 2. Tectonic history of the Coramup Gneiss and a kinematic framework for Mesoproterozoic collision of the West Australian and Mawson cratons. J. Metamorph. Geol. 22, 713–731.
Brewer, T.S., Atkin, B.P., 1987. In: Geochemical and Tectonic Evolution of the Proterozoic Telemark Supracrustals, Southern Norway, vol. 33. Geological Society, London, Special Publications, pp. 471–487.
Brewer, T.S., Menuge, J.F., 1998. Metamorphic overprinting of Sm-Nd isotopic systems in volcanic rocks: the Telemark supergroup, southern Norway. Chem. Geol. 145, 1–16.
Camacho, A., Lee, J.K.W., Fitz Gerald, J.D., Zhao, J., Abdu, Y.A., Jenkins, D.M., Hawthorne, F.C., Kyser, T.K., Creaser, R.A., Armstrong, R., Heaman, L.W., 2012. Planar defects as Ar traps in trioctahedral micas: a mechanism for increased Ar retentivity in phlogopite. Earth Planet Sci. Lett. 341–344, 255–267.
Connelly, J.N., Berglund, J., Larson, S.Å., 1996. Thermotectonic evolution of the Eastern Segment of southwestern Sweden: tectonic constraints from U-Pb geochronology. Geol. Soc. London, Spec. Publ. 112, 297–313.
Corfu, F., Larsen, B.T., 2020. U-Pb systematics in volcanic and plutonic rocks of the Krokskogen area: resolving a 40 million years long evolution in the Oslo Rift. Lithos 376–377, 105755.
Cosca, Michael A., Mezger, K., Essene, Eric J., 1998. The Baltica-Laurentia Connection: Sveconorwegian (Grenvillian) metamorphism, cooling, and unroofing in the Bamble sector, Norway. J. Geol. 106, 539–552.
Dahlgren, S., Corfu, F., Heaman, L.M., 1996. U-Pb isotopic time constraints, and Hf and Pb source characteristics of the Larvik plutonic complex, Oslo paleorift. In: Geodynamic and Geochemical Implications for the Rift Evolution, Goldschmidt Conference. Cambridge Publications, Heidelberg, p. 120.
de Haas, G.-J.L.M., Nijland, T.G., Andersen, T., Corfu, F., 2002. New constraints on the timing of deposition and metamorphism in the Bamble sector, south Norway: zircon and titanite U-Pb data from the Nelaug area. GFF 124, 73–78.
Dunlap, W.J., Fossen, H., 1998. Early Paleozoic orogenic collapse, tectonic stability, and late Paleozoic continental rifting revealed through thermochronology of K-feldspars, southern Norway. Tectonics 17, 604–620.
Eliasson, T., Schöberg, H., 1991. U-Pb dating of the post-kinematic Sveconorwegian (Grenvillian) Bohus granite, SW Sweden: evidence of restitic zircon. Precambrian Res. 51, 337–350.
Engvik, A.K., Bingen, B., Solli, A., 2016. Localized occurrences of granulite: P–T modeling, U–Pb geochronology and distribution of early-Sveconorwegian high-grade metamorphism in Bamble, South Norway. Lithos 240–243, 84–103.
Engvik, A.K., Corfu, F., Solli, A., Austrheim, H., 2017. Sequence and timing of mineral replacement reactions during albitisation in the high-grade Bamble lithotectonic domain, S-Norway. Precambrian Res. 291, 1–16.
Goscombe, B.D., Gray, D.R., 2008. Structure and strain variation at mid-crustal levels in a transpressional orogen: a review of Kaoko Belt structure and the character of West Gondwana amalgamation and dispersal. Gondwana Res. 13, 45–85.
Granseth, A., Slagstad, T., Coint, N., Roberts, N.M.W., Røhr, T.S., Sørensen, B.E., 2020. Tectonomagmatic evolution of the Sveconorwegian orogen recorded in the chemical and isotopic compositions of 1070–920 Ma granitoids. Precambrian Res. 340.
Hageskov, B., 1980. The Sveconorwegian structures of the Norwegian part of the Kongsberg-Bamble-Østfold segment. GFF 102, 150–155.
Hageskov, B., 1985. Constrictional deformation of the Koster dyke swarm in a ductile sinistral shear zone, Koster island, SW Sweden. Bull. Geol. Soc. Den. 34, 151–197.
Holdsworth, R.E., Pinheiro, R.V.L., 2000. The anatomy of shallow-crustal transpressional structures: insights from the Archaean Carajás fault zone, Amazon, Brazil. J. Struct. Geol. 22, 1105–1123.
Holdsworth, R.E., Stewart, M., Imber, J., Strachan, R.A., 2001. The structure and rheological evolution of reactivated continental fault zones: a review and case study. Geol. Soc. London, Spec. Publ. 184, 115–137.
Kellett, D.A., Pehrsson, S., Skipton, D.R., Regis, D., Camacho, A., Schneider, D.A., Berman, R., 2020. Thermochronological history of the northern Canadian Shield. Precambrian Res. 342, 105703.
Kelley, S., 2002. Excess argon in K–Ar and Ar–Ar geochronology. Chem. Geol. 188, 1–22.
Köykkä, J., 2011a. Precambrian alluvial fan and braidplain sedimentation patterns: example from the Mesoproterozoic Rjukan Rift Basin, southern Norway. Sediment. Geol. 234, 89–108.
Köykkä, J., 2011b. The sedimentation and paleohydrology of the Mesoproterozoic stream deposits in a strike–slip basin (Svinsaga Formation), Telemark, southern Norway. Sediment. Geol. 236, 239–255.
Köykkä, J., Lamminen, J., 2011. Tidally influenced clastic epeiric sea at a Mesoproterozoic continental margin, Rjukan Rift Basin, southern Norway. Precambrian Res. 185, 164–182.
Lamminen, J., 2011. Provenance and correlation of sediments in Telemark, South Norway: status of the Lifjell Group and implications for early Sveconorwegian fault tectonics. Norw. J. Geol. 91, 57–75.
Lamminen, J., Andersen, T., Nystuen, J.P., 2011. Zircon U-Pb ages and Lu-Hf isotopes from basement rocks associated with Neoproterozoic sedimentary successions in the Sparagmite Region and adjacent areas, South Norway: the crustal architecture of western Baltica. Norwegian J. Geol. Norsk Geologisk Forening 91.
Lamminen, J., Köykkä, J., 2010. The provenance and evolution of the Rjukan Rift Basin, Telemark, south Norway: the shift from a rift basin to an epicontinental sea along a Mesoproterozoic supercontinent. Precambrian Res. 181, 129–149.
Larson, S.Å., Cornell, D.H., Armstrong, R.A., 1999. Emplacement ages and metamorphic overprinting of granitoids in the Sveconorwegian Province in Varmland, Sweden - an ion probe study. Nor. Geol. Tidsskr. 79, 87–95.
Laurent, A.T., Bingen, B., Duchene, S., Whitehouse, M.J., Seydoux-Guillaume, A.-m., Bosse, V., 2018. Decoding a protracted zircon geochronological record in ultrahigh temperature granulite, and persistence of partial melting in the crust, Rogaland, Norway. Contrib. Mineral. Petrol. 173, 29.
Lee, J.-Y., Marti, K., Severinghaus, J.P., Kawamura, K., Yoo, H.-S., Lee, J.B., Kim, J.S., 2006. A redetermination of the isotopic abundances of atmospheric Ar. Geochem. Cosmochim. Acta 70, 4507–4512.
Laajoki, K., Corfu, F., Andersen, T., 2002. Lithostratigraphy and U-Pb geochronology of the Telemark supracrustals in the Bandak-Sauland area, Telemark, south Norway. Norw. J. Geol. 119–138, 2002.
McDougall, I., Harrison, T.M., 1999. Geochronology and Thermochronology by the $^{40}Ar/^{39}Ar$ Method, second ed. Oxford Univ. Press, Oxford.
Mulch, A., Cosca, M.A., Andresen, A., Fiebig, J., 2005. Time scales of deformation and exhumation in extensional detachment systems determined by high-spatial resolution in situ UV-laser 40Ar/39Ar dating. Earth Planet Sci. Lett. 233, 375–390.
Munz, I.A., 1990. Whiteschists and orthoamphibole-cordierite rocks and the P-T-t path of the Modum Complex, south Norway. Lithos 24, 181–199.
Munz, I.A., Morvik, R., 1991. Metagabbros in the Modum Complex, southern Norway: an important heat source for Sveconorwegian metamorphism. Precambrian Res. 52, 97–113.
Munz, I.A., Wayne, D., Austrheim, H., 1994. Retrograde fluid infiltration in the high-grade Modum Complex South Norway: evidence for age, source and REE mobility. Contrib. Mineral. Petrol. 116, 32–46.
Möller, C., Andersson, J., 2018. Metamorphic zoning and behaviour of an underthrusting continental plate. J. Metamorph. Geol. 36, 567–589.
Möller, C., Andersson, J., Dyck, B., Antal Lundin, I., 2015. Exhumation of an eclogite terrane as a hot migmatitic nappe, Sveconorwegian orogen. Lithos 226, 147–168.
Neumann, H., 1960. Apparent ages of Norwegian minerals and rocks. Norw. J. Geol. 40, 173–191.
Nijland, T.G., Harlov, D.E., Andersen, T., 2014. The Bamble sector, south Norway: a review. Geosci. Front. 5, 635–658.
Nordgulen, Ø., 1999. Bedrock Map HAMAR, Geologisk Kart over Norge. NGU, Trondheim.
Page, L.M., Möller, C., Johansson, L., 1996a. 40Ar39Ar geochronology across the mylonite zone and the southwestern granulite province in the Sveconorwegian orogen of S Sweden. Precambrian Res. 79, 239–259.
Page, L.M., Stephens, M.B., Wahlgren, C.-H., 1996b. 40Ar/39Ar geochronological constraints on the tectonothermal evolution of the Eastern Segment of the Sveconorwegian Orogen, south-central Sweden. Geol. Soc. London, Spec. Publ. 112, 315–330.
Park, R.G., Åhäll, K.I., Bland, M.P., 1991. The Sveconorwegian shear-zone network of SW Sweden in relation to mid-Proterozoic plate movements. Precambrian Res. 49, 245–260.
Pedersen, L.E., Heaman, L.M., Holm, P.M., 1995. Further constraints on the temporal evolution of the Oslo Rift from precise U-Pb zircon dating in the Siljan-Skrim area. Lithos 34, 301–315.
Renne, P.R., Mundil, R., Balco, G., Min, K., Ludwig, K.R., 2010. Joint determination of ^{40}K decay constants and $^{40}Ar^*/^{40}K$ for the Fish Canyon sanidine standard, and improved accuracy for $^{40}Ar/^{39}Ar$ geochronology. Geochem. Cosmochim. Acta 74, 5349–5367.
Schaen, A.J., Jicha, B.R., Hodges, K.V., Vermeesch, P., Stelten, M.E., Mercer, C.M., Phillips, D., Rivera, T.A., Jourdan, F., Matchan, E.L., Hemming, S.R., Morgan, L.E., Kelley, S.P., Cassata, W.S., Heizler, M.T., Vasconcelos, P.M., Benowitz, J.A., Koppers, A.A.P., Mark, D.F., Niespolo, E.M., Sprain, C.J., Hames, W.E., Kuiper, K.F., Turrin, B.D., Renne, P.R., Ross, J., Nomade, S., Guillou, H., Webb, L.E., Cohen, B.A., Calvert, A.T., Joyce, N., Ganerød, M., Wijbrans, J., Ishizuka, O., He, H., Ramirez, A., Pfänder, J.A., Lopez-Martínez, M., Qiu, H., Singer, B.S., 2020. Interpreting and reporting 40Ar/39Ar geochronologic data. GSA Bulletin 133, 461–487.
Scheiber, T., Viola, G., Bingen, B., Peters, M., Solli, A., 2015. Multiple reactivation and strain localization along a Proterozoic orogen-scale deformation zone: the

Kongsberg-Telemark boundary in southern Norway revisited. Precambrian Res. 265, 78–103.
Scheiber, T., Viola, G., Wilkinson, C.M., Ganerød, M., Skår, Ø., Gasser, D., 2016. Direct 40Ar/39Ar dating of late Ordovician and Silurian brittle faulting in the southwestern Norwegian Caledonides. Terra. Nova 28, 374–382.
Slagstad, T., Marker, M., Roberts, N.M.W., Saalmann, K., Kirkland, C.L., Kulakov, E., Ganerød, M., Røhr, T.S., Møkkelgjerd, S.H.H., Granseth, A., Sørensen, B.E., 2020. The Sveconorwegian orogeny – Reamalgamation of the fragmented southwestern margin of Fennoscandia. Precambrian Res. 350, 105877.
Slagstad, T., Roberts, N.M., Coint, N., Høy, I., Sauer, S., Kirkland, C.L., Marker, M., Røhr, T.S., Henderson, I.H., Stormoen, M.A., 2018. Magma-driven, high-grade metamorphism in the Sveconorwegian Province, southwest Norway, during the terminal stages of Fennoscandian Shield evolution. Geosphere 14, 861–882.
Spencer, C.J., Roberts, N.M.W., Cawood, P.A., Hawkesworth, C.J., Prave, A.R., Antonini, A.S.M., Horstwood, M.S.A., 2014. Intermontane basins and bimodal volcanism at the onset of the Sveconorwegian Orogeny, southern Norway. Precambrian Res. 252, 107–118.
Starmer, I.C., 1993. The Sveconorwegian orogeny in Southern Norway, relative to deep-crustal structures and events in the Nort-Atlantic Proterozoic supercontinent. Nor. Geol. Tidsskr. 73, 109–132.
Stephens, M.B., Bergström, U., Wahlgren, C.-H., 2020. In: Regional Context and Lithotectonic Framework of the 1.1–0.9 Ga Sveconorwegian Orogen, Southwestern Sweden, vol. 50. Geological Society, London, Memoirs, pp. 337–349.
Stephens, M.B., Wahlgren, C.-H., Weijermars, R., Cruden, A.R., 1996. Left-lateral transpressive deformation and its tectonic implications, Sveconorwegian orogen, Baltic Shield, southwestern Sweden. Precambrian Res. 79, 261–279.
Stübner, K., Warren, C., Ratschbacher, L., Sperner, B., Kleeberg, R., Pfänder, J., Grujic, D., 2017. Anomalously old biotite 40Ar/39Ar ages in the NW Himalaya. Lithosphere 9, 366–383.
Ulmius, J., Möller, C., Page, L., Johansson, L., Ganerød, M., 2018. The eastern boundary of Sveconorwegian reworking in the Baltic Shield, defined by 40Ar/39Ar geochronology across the southernmost Sveconorwegian Province. Precambrian Res. 307, 201–217.
Vander Auwera, J., Bolle, O., Bingen, B., Liégeois, J.P., Bogaerts, M., Duchesne, J.C., De Waele, B., Longhi, J., 2011. Sveconorwegian massif-type anorthosites and related granitoids result from post-collisional melting of a continental arc root. Earth Sci. Rev. 107, 375–397.
Villa, 1998. Isotopic closure. Terra. Nova 10, 42–47.
Viola, G., Bingen, B., Solli, A., 2016. Bedrock geology map of the Kongsberg lithotectonic unit, Kongsberg - Modum - Hønefoss. Geol. Surv. Norway. Scale 1:100 000, 1 sheet.
Viola, G., Henderson, I.C., 2010. Inclined transpression at the toe of an arcuate thrust: an example from the Precambrian 'Mylonite Zone' of the Sveconorwegian orogen. Geol. Soc. London, Spec. Publ. 335, 715–737.
Viola, G., Henderson, I.H.C., Bingen, B., Hendriks, B.W.H., 2011. The Grenvillian–Sveconorwegian orogeny in Fennoscandia: back-thrusting and extensional shearing along the "mylonite zone". Precambrian Res. 189, 368–388.
Viola, G., Henderson, I.H.C., Bingen, B., Thomas, R.J., Smethurst, M.A., de Azavedo, S., 2008. Growth and collapse of a deeply eroded orogen: insights from structural, geophysical, and geochronological constraints on the Pan-African evolution of NE Mozambique. Tectonics 27, TC5009.
Viola, G., Venvik Ganerød, G., Wahlgren, C.-H., 2009. Unraveling 1.5 Ga of brittle deformation history in the Laxemar-Simpevarp area, southeast Sweden: a contribution to the Swedish site investigation study for the disposal of highly radioactive nuclear waste. Tectonics 28.
Wang, X.D., Söderlund, U., Lindh, A., Johansson, L., 1998. U–Pb and Sm–Nd dating of high-pressure granulite- and upper amphibolite facies rocks from SW Sweden. Precambrian Res. 92, 319–339.
Warren, C.J., Hanke, F., Kelley, S.P., 2012. When can muscovite 40Ar/39Ar dating constrain the timing of metamorphic exhumation? Chem. Geol. 291, 79–86.
Yang, J.-H., Wu, F.-Y., Chung, S.-L., Lo, C.-H., Wilde, S.A., Davis, G.A., 2007. Rapid exhumation and cooling of the Liaonan metamorphic core complex: inferences from 40Ar/39Ar thermochronology and implications for Late Mesozoic extension in the eastern North China Craton. Geol. Soc. Am. Bull. 119, 1405–1414.